Pergamon

Int. J. Solids Structures Vol. 34, No. 19, pp. 2393–2428, 1997

0020-7683/97 $17.00 + .00

PII: S0020-7683(96)00172-2

INDENTATION OF SOLIDS WITH GRADIENTS IN ELASTIC PROPERTIES: PART II. AXISYMMETRIC INDENTORS

A. E. GIANNAKOPOULOS and S. SURESH†
Department of Materials Science and Engineering, Massachusetts Institute of Technology, Cambridge, MA 02139, U.S.A.

(*Received* 18 *April* 1996; *in revised form* 2 *August* 1996)

Abstract—Analytical and computational results are presented for the evolution of stresses and deformation fields due to indentation from a rigid axisymmetric indentor on an elastic substrate. The theory addresses the variations in Young's modulus, E, of the substrate as a function of depth, z, beneath the indented surface for two cases: (1) a simple power law, $E = E_0 z^k$, where $0 \leqslant k < 1$ is a non-dimensional exponent; (2) an exponential law, $E = E_0 e^{\alpha z}$, where E_0 is Young's modulus at the surface and α is a length parameter. The indentor geometries for which analytic solutions are derived include flat circular punch, sphere and circular cone. The analytical results for the punch are compared with finite element simulations; the latter validate the theory and offer further insights into the effects of the variation in Poisson ratio, ν, with depth. © 1997 Elsevier Science Ltd.

1. INTRODUCTION

The indentation due to the application of a point force of an elastic solid, with gradients in Young's modulus as a function of depth, was analyzed in Part I of this work (Giannakopoulos and Suresh, 1997). Closed-form solutions and computational results were presented in Part I for the stresses and displacement fields in the elastic medium which was assumed to have a fixed Poisson ratio and whose Young's modulus, E, varied with depth, z, beneath the indented surface by one of two prescribed functions: (1) a simple power law, $E = E_0 z^k$, where $0 \leqslant k < 1$ is a non-dimensional exponent, and (2) an exponential law, $E = E_0 e^{\alpha z}$, where E_0 is Young's modulus at the surface and $\alpha < 0$ and $\alpha > 0$ denote hardened and softened surfaces, respectively. The effect of Poisson ratio on the evolution of fields during indentation by a point force were also studied computationally.

A survey of published work reveals that little understanding exists about the evolution of stresses and displacements as a function of depth in the graded medium beneath the contact surface, for axisymmetric indentors. (A full review of literature on the indentation of a graded elastic solid by a point force is given in Part I.) For the power-law variation of E with depth, $E = E_0 z^k$, Kassir (1972) presented solutions for *surface displacements* due to a rigid circular punch under normal and shear loads. He considered the special case of the critical Poisson ratio, $\nu = \nu_{cr} = 1/(k+2)$. (As shown in Part I, at $\nu = \nu_{cr}$ is a special case where radial stress fields emanate from the point of indentation.) Booker *et al.* (1985) reported solutions for the *vertical surface displacements* of a graded elastic half-space under point, line, circular ring and strip loads applied normally to the surfaces. They considered only a specific Poisson ratio, $\nu = 0.25$, and did not examine general axisymmetric indentor geometries or exponent rise or decay in E as a function of depth. Oner (1990) analyzed the surface displacements arising from rigid circular and rectangular punches (footings) which indented a graded elastic substrate with a power law variation of E. He considered only the case of $\nu = \nu_{cr} = 1/(k+2)$. Similar analyses were also reported by Fabrikant (1989) and Yong and Hanson (1994).

It is the objective of the present paper, Part II, to provide analytical and computational solutions for more general and practically relevant problems of indentation of a graded elastic substrate by rigid axisymmetric indentors. The indentor geometries examined include

† Author to whom correspondence should be addressed.

a circular punch, a sphere and a cone. The variations of the Young's modulus with depth beneath the indented surface were close to be the same as those in Part I, i.e., a power law function and an exponential function. The Poisson ratio was held constant (as a function of depth); however, several Poisson ratios were examined ($0 \leqslant \nu < 1/2$). (This choice was motivated by the results of Part I that gradients in Poisson ratio have a significantly less pronounced response on the indentation characteristics of the elastic substrate than gradients in Young's modulus.) The analytical results for indentation of a grated elastic solid by a rigid circular punch are compared with detailed finite element simulations. Similar computational results for the conical and spherical indentors are not reported here because of space restrictions; they will be presented separately, along with the results of systematic experimental measurements (Suresh *et al.*, 1996; Alcala *et al.*, 1996). In all subsequent analyses (r, z) denotes the axisymmetric polar coordinates for a half space, $z \geqslant 0$, with corresponding displacements (u, w). A force, P, is applied on the indentor normal to the surface and the problem becomes axisymmetric around the z-axis.

2. THEORY FOR THE RIGID CIRCULAR PUNCH PROBLEM

2.1. *The power law case*: $E = E_0 z^k$

Using the solution of the generic Boussinesq problem (a point force on the surface of a semi-infinite elastic medium), a circular punch of radius a can be analyzed, Fig. 1a. Let $p(r)$ be the normal pressure at the contact circular area with $p(r) \geqslant 0$ for $0 \leqslant r \leqslant a$ and $p(r) = 0$ for $r > a$. Since the contact is assumed frictionless, no surface shear stresses are present, $\sigma_{rz}(z = 0) = 0$. The vertical displacement at the surface is $w(r) = w_0$ at $0 \leqslant r \leqslant a$. Using the expressions for the point load (see Part I), the integral equations for a ring type of normal load and subsequently for a uniform, normal to the surface $z = 0$, axisymmetric pressure was formulated. The solution to the rigid, frictionless indentor problem involves a system of coupled integral equations of the form

$$0 = \int_0^\infty p(\beta) \int_{J_0} (\beta r/a)\, \mathrm{d}\beta, \tag{1}$$

for the condition of no external stress outside the contact area ($1 < r/a < \infty$), and

$$\frac{w_0}{A_k} = \int_0^\infty \beta^{k-1} p(\beta) \int_{J_0} (\beta r/a)\, \mathrm{d}\beta, \tag{2}$$

for the condition of the punch displacement inside the contact area ($0 \leqslant r/a < 1$). Here, J_0 is the Bessel function of the first kind of zeroth order and A_k is a constant that appears at the force-depth relation of the point force solution (Booker *et al.*, 1985; Giannakopoulos and Suresh, 1996). The general solution of the above system of equations, for $0 \leqslant k < 1$, is (Busbridge, 1938)

$$p(r/a) = \frac{w_0}{A_k} (2r/a)^{-k/2+3/2} \int_0^1 t^{k/2+1/2} J_{(k-1)/2}(tr/a)\, \mathrm{d}t \int_0^1 t(1-t^2)^{k/2-3/2}\, \mathrm{d}t. \tag{3}$$

Using the integral properties of the Bessel functions (Whittaker and Watson, 1962), we obtain the result

$$p(r) = \frac{w_0}{A_k} \frac{2^{1-k}}{[\Gamma(k/2+1/2)]^2} (a^2 - r^2)^{(k-1)/2}, \tag{4}$$

where $\Gamma(\ )$ is the Gamma function (Magnus and Oberhettinger, 1954). A similar result was derived by Mossakovskii (1958). Note that the homogeneous elastic substrate case is

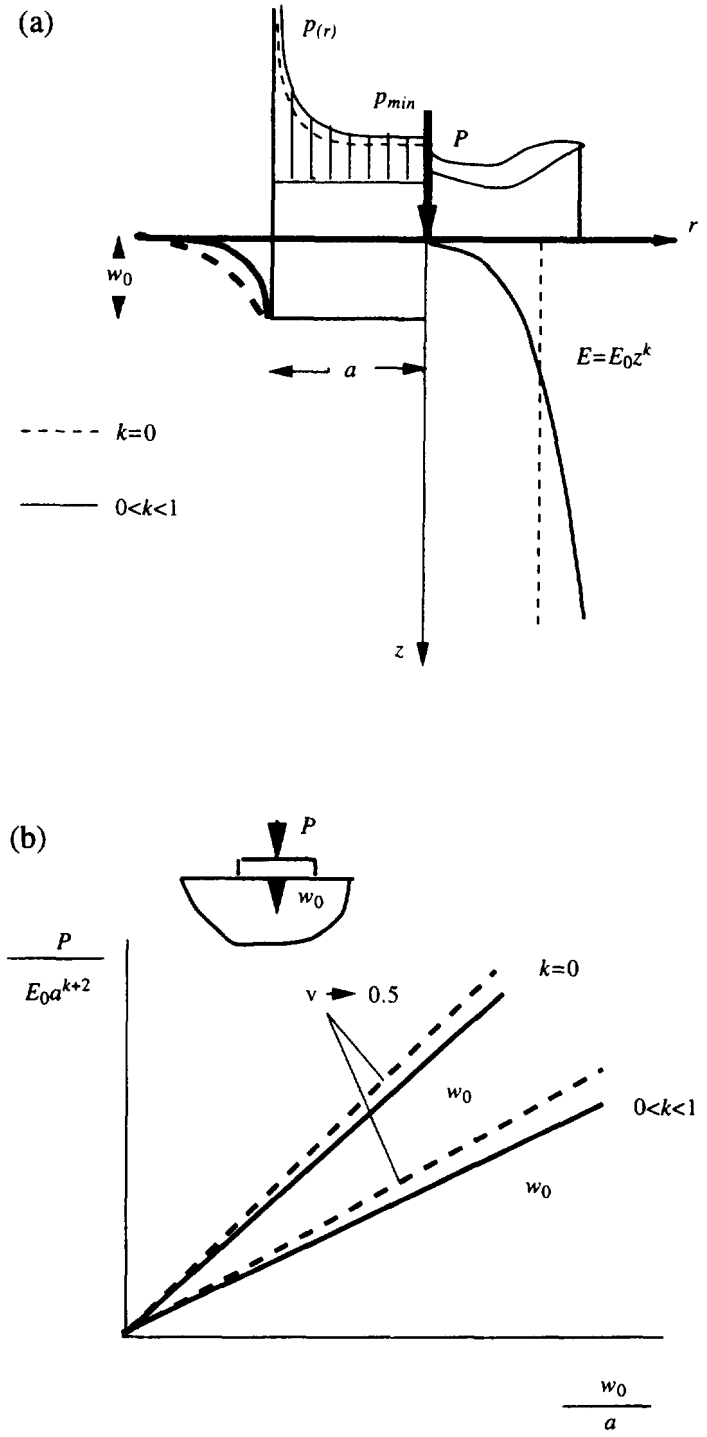

Fig. 1. (a) The circular punch problem for the power law case, $E = E_0z^k$. (b) The normalized force-depth $(P/(E_0a^{k+2}) - w_0/a)$ relation for the homogeneous and power law cases.

retrived for $k = 0$ (Sneddon, 1946). The singularity at the punch edge ($r = a$) is weaker for the graded elastic medium than that for the homogeneous case. For the same indentation depth, w_0, the pressure distribution is also correspondingly lower at all points of contact ($0 \leqslant r \leqslant a$). The contact pressure distribution decreases with the Poisson ratio, ν, for the same indentation depth. It is clear that the problem's only characteristic length is the radius, a, of contact. Taking into account the actual relation for the constant, A_k, and integrating for the total applied force, P,

$$p(r) = \frac{P(1+k)}{2\pi a^2}\left(1-\frac{r^2}{a^2}\right)^{(k-1)/2}. \tag{5}$$

The minimum contact pressure appears at $r = 0$,

$$p_{\min} = p(0) = \frac{P(1+k)}{2\pi a^2}, \tag{6}$$

and, for a given load, P, is higher than the corresponding homogeneous elastic case by a factor of k. The displacement, w_0, is related to the total load, P, according to

$$w_0 = \frac{\pi\theta^*}{\cos\dfrac{k\pi}{2}}\frac{P(1+k)}{2a^{1+k}}, \tag{7}$$

where

$$\theta^* = \frac{(1-\nu^2)}{E_0}\frac{Cq\sin\dfrac{\pi q}{2}}{2(1+k)\sqrt{\pi}}\frac{\Gamma\left(\dfrac{1+k}{2}\right)}{\Gamma\left(1+\dfrac{k}{2}\right)}, \tag{8}$$

with

$$q = \sqrt{(1+k)(1-k\nu/(1-\nu))}, \quad C = \frac{2^{1+k}\Gamma\left(\dfrac{3+k+q}{2}\right)\Gamma\left(\dfrac{3+k-q}{2}\right)}{\pi\Gamma(2+k)}. \tag{9}$$

Note that the force-depth $(P-w_0)$ relation is linear, as in the homogeneous case; however, the force is lower than the corresponding homogeneous case, as indicated schematically in Fig. 1b. The displacement outside the contact region, $0 \leqslant r < \infty$, is

$$w(r) = \frac{\theta^* P}{r^{k+1}}F\left(\frac{k+1}{2}, \frac{k+1}{2}, \frac{k+3}{2}, \frac{a^2}{r^2}\right), \tag{10}$$

where F is the Gauss hypergeometric function (Magnus and Oberhettinger, 1954). For the same indentation depth, w_0, less sinking-in appears for the elastic solid with a power law variation of E than for the corresponding homogeneous one. The same results were found by Booker *et al.* (1985) in a different way: by using the point force solution in spherical coordinates, representing the punch deflection by a Fourier integral and finally solving the resulting Abel integral equation. For $k = 0$ $(q = 1)$, that is, $E = E_0$, we recover the classic homogeneous solution of Sneddon (1946) with

$$\theta^* = \frac{1-\nu^2}{\pi E_0}, \quad F\left(\frac{1}{2}, \frac{1}{2}, \frac{3}{2}, \frac{a^2}{r^2}\right) = \frac{r}{a}\sin^{-1}\left(\frac{a}{r}\right). \tag{11}$$

For $\nu = 1/(2+k)$, which gives $q = 1$, θ^* simplifies to

$$\theta^* = \frac{1-\nu^2}{\pi E_0} \frac{2^k \Gamma\left(\frac{1+k}{2}\right)}{(1+k)\sqrt{\pi}}. \tag{12}$$

This particular case was examined by Kassir (1972) where the solution for the force-depth relation becomes

$$w_0 = \frac{(1+\nu)}{\cos\frac{k\pi}{2}} \frac{P}{4E_0 a^{1+k}}. \tag{13}$$

Some of Kassir's results (valid for $\nu = 1/(2+k)$) are $w_0 E_0 a^{1+k}/(2P(1+\nu)) = 0.3927, 0.4535, 0.5554, 0.7854$, for $k = 0, 1/3, 1/2, 1/3$, respectively. On similar lines, one can use the closed form point force solution for the particular case of Poisson ratio $\nu = 1/(k+2)$ to construct a solution for rigid square punches of length B, as was done by Oner (1990),

$$w_0 = \frac{2(1+\nu)}{E_0} \frac{P}{B^{1+k}} K, \tag{14}$$

with the constant $K = 0.2165, 0.2912, 0.3841, 0.5945$ for $k = 0, 1/3, 1/2, 2/3$, respectively. The above solution is particularly important for the unloading interpretation of the Vickers and other sharp indentation tests (e.g., Berkovich, Rockwell, etc.).

2.2. *The exponential law case*: $E = E_0 e^{\alpha z}$

In the following, in order to keep the analysis short without sacrificing the essential results, we examined the particular case of $\nu = 0$. In this case, an approximate closed form analytic solution can be derived which can be very illuminating for the subsequent discussions of the influence of material length in graded materials. Full finite element analysis (presented later) showed that this assumption is not very limiting regarding the essential results. From Part I, one can use the point force solution for $\nu \neq 0$ in the same way as below; however, the analysis becomes unduly complicated. Using the force-surface displacement relation from the Boussinesq point force problem, Part I, Giannakopoulos and Suresh (1996), the surface displacement for a unit ring load, at a distance ρ from the z-axis of symmetry is given by

$$w(r,\rho) = \frac{\rho}{E_0} \int_0^\infty G(t/\alpha) J_0(r/q) J_0(\rho t)\, \mathrm{d}t, \tag{15}$$

where

$$G(q/\alpha) = \frac{(2q/\alpha)\sqrt{(2q/\alpha)^2+1}}{(1+\sqrt{(2q/\alpha)^2+1})^2}. \tag{16}$$

Assume an axisymmetric convex indentor, $z_1(r)$, in perfect frictionless contact with the surface within a disk of radius a. Let $p(r)$ be the contact pressure ($p(r) \geqslant 0$) and h the indentor's depth. Then, the integral equation that controls the problem for $0 \leqslant r \leqslant a$ reads as

$$\int_0^a w(r,\rho) p(\rho)\, \mathrm{d}\rho = h - z_1(r). \tag{17}$$

The integral equation (17) does not have an exact solution, but may be solved approximately. We first observe that $G(x)$ is bounded, $0 \leqslant G(x) < 1$, with $G(x=0) = 0$ and $G(x \to$

$\infty) \to 1$. The tangent line around $x = 0$ is $G(x) = x/2$, $0 \leqslant G < 1$. The problem can be normalized by taking the non-dimensional quantities

$$x = r\alpha, \quad \xi = \rho\alpha, \quad \alpha^* = a\alpha, \quad p(r) = \alpha\phi(r\alpha). \tag{18}$$

Note that α^* gives the relative size of the contact radius, a, and the material characteristic length is $1/\alpha$. Then, the controlling integral equation (17) can be rearranged as

$$\int_0^{\alpha^*} K(x,\xi)\xi\phi(\xi)\,\mathrm{d}\xi = f(x), \tag{19}$$

in the region $0 \leqslant \xi \leqslant \alpha^*$, with

$$f(x) = E_0(h - z_1(x)), \quad K(x,\xi) = \int_0^{\infty} G(s)J_0(xs)J_0(\xi s)\,\mathrm{d}s. \tag{20}$$

In view of the shape of function $G(s)$, the kernel, $K(x,\xi)$, can be approximated as

$$K(x,\xi) \approx \int_0^{\infty} J_0(xs)J_0(\xi s)\,\mathrm{d}s - \int_0^{A} (1 - G(s))J_0(xs)J_0(\xi s)\,\mathrm{d}s, \tag{21}$$

with A being a dimensionless constant with a value sufficiently high to capture the essentials of the approximation (21). Expanding the Bessel functions into power series and keeping N terms in the integrations of the series expansions, we obtain

$$K(x,\xi) \approx \int_0^{\infty} J_0(xs)J_0(\xi s)\,\mathrm{d}s - \sum_{k=0}^{N} \frac{(-1)^k C_k M_k(x,\xi)}{4^k (K!)^2}, \tag{22}$$

with

$$M_k(x,\xi) = \sum_{j=0}^{k} \binom{k}{j}^2 x^{2(k-j)}\xi^{2j}, \quad C_k = \int_0^{A} (1 - G(s))s^{2k}\,\mathrm{d}s. \tag{23}$$

From the functional form of $G(x)$, it can be concluded that $C_k > 0$. Numerical integration gives the following results: $C_0 = 3.7$ and $C_1 = 403.5$. A further transformation,

$$t = x/\alpha^*, \quad \chi(t) = \alpha^*\phi(\alpha^* t), \tag{24}$$

gives (for the range $0 \leqslant t \leqslant 1$)

$$\alpha^* \int_0^{1} K(t\alpha^*, \tau\alpha^*)\tau\chi(\tau)\,\mathrm{d}\tau = f(t\alpha^*). \tag{25}$$

For the circular stamp case, the solution and the Bessel function, J_0, are expanded in Legendre polynomials, P_n. Extracting the singular term of the homogeneous circular punch problem (a procedure typical for elastic fracture mechanics),

$$\chi(t) = \frac{1}{\sqrt{(1-t^2)}} \sum_{m=0}^{\infty} Y_m P_m^*(t), \tag{26}$$

where Y_m ($m = 0, 1, 2, \ldots$) are constants to be determined and P_m^* are connected with the Legendre polynomials, P_{2m}, $P_m^*(t) = P_{2m}(\sqrt{1-t^2})$.

Using the orthogonality of the Legendre polynomials and the integral properties of the Bessel functions, we can find iteratively the constants, Y_m. Remembering that $p(r) = \chi(r/a)/a$, the total force, P, acting on the indentor is

$$P = 2\pi \int_0^a rp(r)\,\mathrm{d}r = 2\pi a Y_0. \tag{27}$$

In order to determine the depth-contact radius $(h-a)$ relation for sufficiently smooth indentors, we assume complete contact and zero contact stress at the contact perimeter $r = a$ $(t = 1)$.

For $N = 1$, we have a two-term expansion given by the two constants

$$Y_0 = F_0/\psi(\alpha^*), \quad Y_1 = Y_0 X_1 + F_1, \tag{28}$$

where

$$\psi(\alpha^*) = \frac{\pi}{2} - \alpha^*\left(C_0 - \frac{C_1}{3}\alpha^{*2} + \frac{2}{45\pi}C_1^2\alpha^{*5}\right), \tag{29}$$

$$F_0 = f_0 + \frac{4}{3\pi}C_1 f_1 \alpha^{*3}, \quad F_1 = \frac{40}{\pi}f_1, \tag{30}$$

$$f_l = \int_0^1 \frac{f(t\alpha^*)P_l^*(t)}{\sqrt{1-t^2}}\,t\,\mathrm{d}t, \quad (l = 0, 1, \ldots), \tag{31}$$

$$X_0 = 1, \quad X_1 = \frac{4C_1}{3\pi}\alpha^{*3}. \tag{32}$$

It is implicitly assumed that the previous expansions hold for small values of $\alpha^*(|\alpha^*| \ll 1)$.

Some closed form approximations can be made for *stamps* with a *circular* base of radius a, Fig. 2a. It may then be assumed that $z_1(r) = w_0$ in eqns (17), (20a) and (31), an assumption that will be further discussed later. The pressure distribution, $p(r)$ $(0 \leqslant r \leqslant a)$, is related to the load as

$$p(r) \approx \frac{P}{2\pi a^2}\left(1 - \frac{r^2}{a^2}\right)^{-1/2}\left\{1 + \frac{C_1}{\pi}\alpha^{*3}\left(\frac{4}{3} - 2\frac{r^2}{a^2}\right)\right\}. \tag{33}$$

Note that the ordinary square root singularity of the contact pressure distribution is retained, as in the homogeneous case $(\alpha = 0)$. For a given indentation depth, w_0, the contact pressure is higher for $\alpha > 0$ (soft to stiff case) and lower for $\alpha < 0$ (stiff to soft case) than the corresponding homogeneous case $(\alpha = 0)$ when the punch is in complete contact with the surface. The case of $\alpha < 0$ is expected on the physical argument that the soft substrate will not resist strongly the applied deformation. However, the case of $\alpha > 0$ contradicts the power law case which also models soft to stiff elastic gradation (eqn (5)). The reason is the way the gradation takes place: concave in the power law case and convex in the exponential case. This seems to be important and is related to the type of constraint in the overall deformation that the functional form of the elastic modulus exerts in the contact problems: the convex type results in higher resistance than the concave type.

Using eqn (27) in eqn (17) (with $z_1 = 0$ and $h = w_0$), the force-depth $(P = w_0)$ relation for the circular punch reduces to

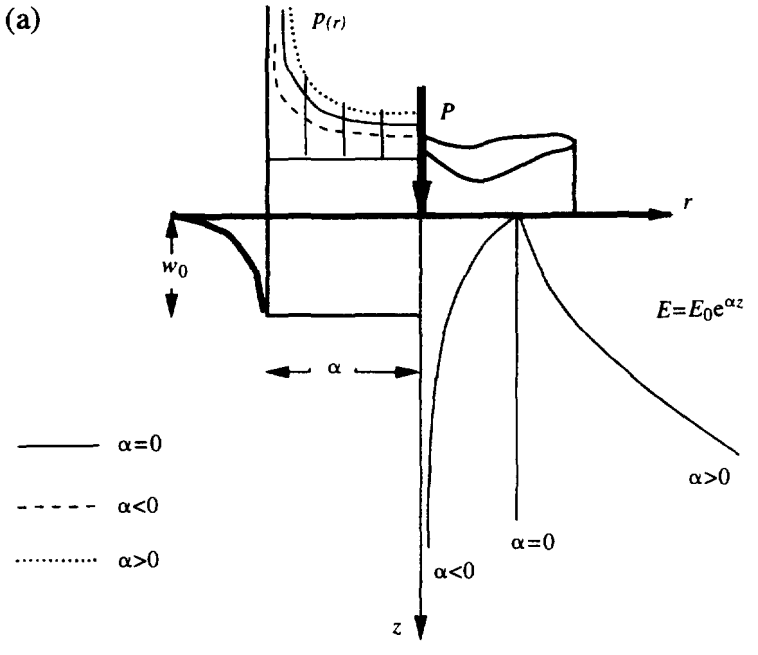

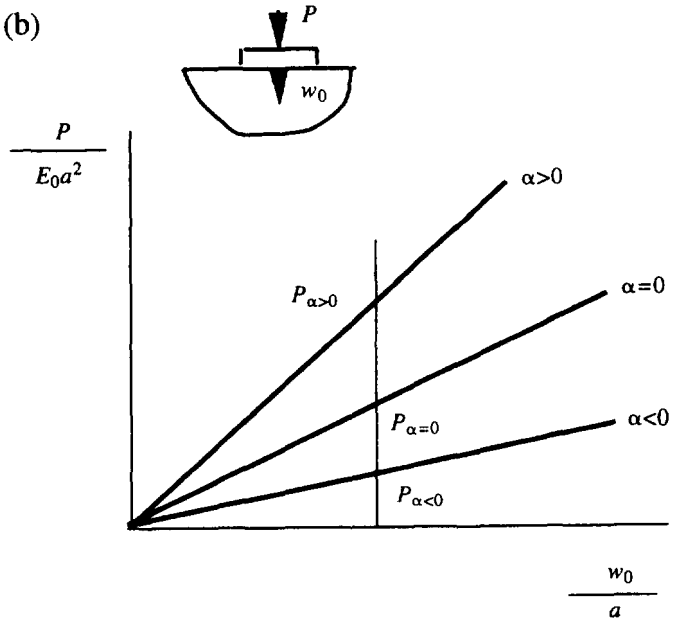

Fig. 2. (a) The circular punch problem for the exponential law case, $E = E_0 e^{\alpha z}$. (b) The normalized force-depth $(P/(E_0 a^2) - w_0/a)$ relation for the homogeneous and exponential law cases.

$$w_0 \approx \frac{P}{\pi a E_0}\left\{\frac{\pi}{2} - \alpha^*\left(C_0 - C_1\frac{\alpha^{*2}}{3} + C_1^2\frac{2}{45\pi}\alpha^{*5}\right)\right\}. \tag{34}$$

The force-depth $(P - w_0)$ relation is linear, as in the homogeneous case ($\alpha = 0$); however, the force is higher for $\alpha > 0$ and lower for $\alpha < 0$, as indicated in Fig. 2b. For the same absolute value of α, and normalized depth w_0/a, the force drop for $\alpha < 0$ is higher than the corresponding force increase for $\alpha > 0$. This means that, if the force is normalized by the

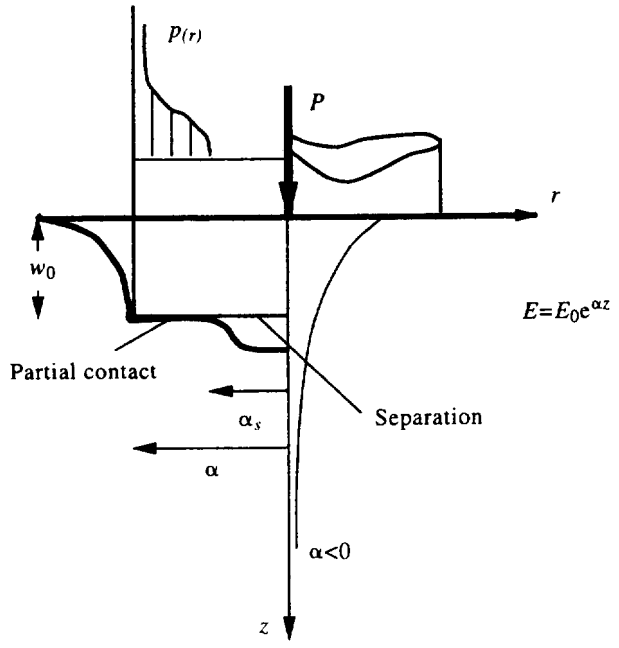

Fig. 3. The development of partial contact for the exponential law case, $E = E_0 e^{\alpha z}$, $a\alpha \leqslant -1.125$.

corresponding value for the homogeneous case, $P_{\alpha=0}$, then $[1-P_{\alpha<0}/P_{\alpha=0}] > P_{\alpha>0}/P_{\alpha=0} > 0$ (see Fig. 3).

3. THE GENERAL RIGID AXISYMMETRIC INDENTOR

3.1. *The power law case*: $E = E_0 z^k$

Using the superposition argument, we can use the previous punch solution to solve the problem of a rigid (frictionless) axisymmetric indentor of convex shape $z_1(r)$. Assume that the contact area is a circular disc of radius $a (0 \leqslant r \leqslant a)$. As a fairly general case of a wide class of indentor shapes, let $z_1(r) = Mr^\beta$, with $\beta \geqslant 1$ and $M > 0$ (the dimension of M is length$^{1-\beta}$). The displacement at contact follows the indentor's shape:

$$w(r) = h - Mr^\beta, \tag{35}$$

where h is the depth of the indentor's penetration. Then the contact stress distribution, $p(r)$, is formulated by superposition (eqn (5))

$$p(r) = \frac{P(1+k)(1+k+\beta)}{2\pi a^2} \int_{r/a}^{1} \left[t^2 - \left(\frac{r}{a}\right)^2 \right]^{(k-1)/2} t^{\beta-1}\, dt. \tag{36}$$

The total force, P, is given by integrating the contact stresses (eqn (36))

$$P = \frac{\pi 2^{2-k} a^{1+k}}{c_1 \Gamma\left(\frac{1+k}{2}\right)} \left\{ \frac{h}{(1+k)\Gamma\left(\frac{1+k}{2}\right)} - \frac{M\Gamma(1+\beta/2)a^\beta}{(1+k+\beta)\Gamma\left(\frac{1}{2}+\frac{k}{2}+\frac{\beta}{2}\right)} \right\}, \tag{37}$$

where the constant c_1 is

$$c_1 = \frac{\Gamma\left(\frac{1-k}{2}\right)}{\Gamma\left(\frac{1+k}{2}\right)} 2^{1-k}\theta^*\pi. \tag{38}$$

The depth-radius $(h-a)$ relation can be found by requiring that stress be zero at the contact perimeter (which is to be expected for smooth axisymmetric indentors),

$$h = Ma^{\beta} \frac{\Gamma\left(\frac{1+k}{2}\right)\Gamma\left(1+\frac{\beta}{2}\right)}{\Gamma\left(\frac{1}{2}+\frac{k}{2}+\frac{\beta}{2}\right)}. \tag{39}$$

This relation also serves as a measure of the amount of sinking-in of the contact region and indicates that for a given indentation depth, h, the contact radius, a, increases with k. This is expected because close to the surface, the stiffness is low. Using the above relations, we can connect the contact radius, a, with the total force, P,

$$a^{1+k+\beta} = \frac{Pc_1}{M2^{2-k}\pi\beta} \frac{(1+k)(1+k+\beta)}{\Gamma\left(1+\frac{\beta}{2}\right)} \Gamma\left(\frac{1+k}{2}\right)\Gamma\left(\frac{1}{2}+\frac{k}{2}+\frac{\beta}{2}\right). \tag{40}$$

Combining eqns (39) and (40), the force-depth $(P-h)$ relation can be found. It can be shown that the $(P-h)$ curve is always concave, for all axisymmetric indentors described by eqn (35). For low values of h, the P values are lower than for the corresponding homogeneous case, and for higher value of h, the P values are higher than for the homogeneous case, in accordance with expectations. Therefore, for given ν, E_0, k, β and M, the elastic contact problem with power law elastic modulus distribution can be completely solved. It should be further noted that a change in the curvature of the indentor's tip by, for example, plastification, may lead to drastic changes of the force-depth, as well as the average pressure results, a fact that must be carefully examined in actual tests where the indentor is allowed to plastically deform.

In case of $\beta = 2n$, where $n = 1, 2, 3, \ldots$, eqn (36) can be solved exactly to give

$$p(r) = \frac{P(1+k)(1+k+2n)}{2\pi a^2}\left[1-\left(\frac{r}{a}\right)^2\right]^{(1+k)/2} \times \left\{\frac{1}{k+2n-1} + \frac{2n-2}{(k+2n-1)(k+2n-3)}\left(\frac{r}{a}\right)^2 + \cdots + \frac{(2n-2)(2n-4)\ldots 6.4.2}{(k+2n-1)(k+2n-3)\ldots(k+3)(k+1)}\left(\frac{r}{a}\right)^{2n-2}\right\}. \tag{41}$$

For the homogeneous case, $k = 0$, the above results (eqns (40) and (41)) reduce to the results of Hill and Storakers (1990).

The normal surface deformation outside the contact area $(a \leqslant r < \infty)$ is

$$w(r) = M\frac{2\cos\frac{k\pi}{2}}{\pi}\frac{\Gamma\left(\frac{1+k}{2}\right)\Gamma\left(1+\frac{\beta}{2}\right)}{\Gamma\left(\frac{k}{2}+\frac{\beta}{2}+\frac{1}{2}\right)}\int_0^a \frac{t^k(a^\beta - t^\beta)}{(r^2-t^2)^{(k+1)/2}}\,dt. \tag{42}$$

Given an indentation depth, h, the surface deformation outside the contact area is less for a power law material than for a homogeneous one. Hence, for the same indentation depth, less sinking-in at the contact perimeter should appear for the power law solid than for the corresponding homogeneous one.

The horizontal displacement, $u(r)$, at the surface ($z = 0$ and $0 \leqslant r \leqslant \infty$) is related to the vertical displacement, $w(r)$, as

$$u(r) = w(r)\frac{2(1+k)}{qk}\frac{\cos\frac{\pi q}{2}}{\sin\frac{\pi q}{2}}\left\{\frac{\Gamma\left(1+\frac{k}{2}\right)}{\Gamma\left(\frac{1+k}{2}\right)}\right\}^2, \tag{43}$$

with $q = \sqrt{(1+k)(1-kv/(1-v))}$ as before. Note that u and w have no other extrema than that at the surface ($z = 0$).

The present solution also satisfies the incremental contact conditions $dP\,dh \geqslant 0$ and $da\,dh \geqslant 0$, with $P = 0$ and $a = 0$ when only $h = 0$.

The particular case of $k = 1$ (Gibson soil, $E = E_0 z$) (Gibson, 1967), and $v = 0.5$ (incompressibility) will be examined in the Appendix.

3.2. *The exponential law case*: $E = E_0 e^{\alpha z}$

Using superposition of the circular punch solution and the conditions of zero stress at the contact boundary ($r = a$), we can approximate the force-depth ($P-h$) and the depth-contact radius ($h-a$) relations for any convex axisymmetric punch of profile $z_1 = z_1(r)$. The force-contact radius relation ($P-a$) reads as

$$P = \frac{2\pi E_0}{\alpha}[h - I(\alpha^*)]\alpha^*\psi^{-1}, \tag{44}$$

where $\alpha^* = a\alpha$, ψ is given by eqn (29) and

$$I(\alpha^*) = \int_0^1 (1-t^2)^{-1/2} z_1(at) \sum_{m=0}^{N=1} X_m P_m^*(t)\,dt, \tag{45}$$

with $P_m^*(t) = P_{2m}(\sqrt{1-t^2})$ denoting the modified Legendre polynomials. The depth-contact radius relation ($h-a$) is given by

$$h = I(\alpha^*) + \frac{\alpha^*}{\psi - \alpha^*\dfrac{\partial\psi}{\partial\alpha^*}}\frac{\partial I}{\partial\alpha^*}. \tag{46}$$

Combining eqns (44) and (46), we can also relate the force, P, with the depth, h (it is not given here because of space restrictions). The force-depth relation is concave for $\alpha > 0$ (surface softer than bulk material) and convex for $\alpha < 0$ (surface stiffer than bulk material). In the case of a smooth indentor and under low levels of load, the force-depth relation deviates little from the corresponding homogeneous case.

3.3. *Stability issues for the exponential law case*: $E = E_0 e^{\alpha z}$

In all previous analysis, we must satisfy $p(r) \geqslant 0$ $(0 \leqslant r \leqslant a)$ in order to keep the present contact analysis valid. For stability of the load-depth $(P-h)$ result, the incremental contact conditions $dh\,da \geqslant 0$, $dh\,dP > 0$ must be satisfied with $P = 0$ and $\alpha = 0$, if and only if $h = 0$. We now examine how these conditions pertain to the punch, spherical and conical indentors.

For the circular punch case, it can be immediately verified that the above contact condition is never violated, if

$$1 + \frac{4}{3}\frac{C_1 \alpha^{*3}}{\pi} > 0. \tag{47}$$

Condition (47) gives $\alpha^* > -0.18$; a failure to meet this condition implies that a partial contact will develop. The condition applies only to the case of $\alpha < 0$ (stiff surface on a soft substrate, such as for a ceramic coating on a metallic substrate with a graded interface), loss of complete contact is never a problem for $\alpha > 0$ (soft surface on a stiff substrate). To keep the load-displacement response stable, the condition

$$\frac{\pi}{2} - \alpha^*\left(C_0 - C_1\frac{\alpha^{*2}}{3} + C_1^2\frac{2}{45\pi}\alpha^{*5}\right) > 0 \tag{48}$$

must be valid. This condition restricts the values of $\alpha^* = a\alpha$; that is, it restricts the punch radius, a, to be a fraction of the characteristic material length, $|\alpha^{-1}|$, that defines the material inhomogeneity. Condition (48) gives $-0.25 < \alpha^* < 0.4$, independently of the load level. It is clear that for $\alpha < 0$, loss of complete contact will precede instability. For $\alpha < 0$, the stability condition corresponds to an overall loss of stiffness in the circular flat punch test. For $\alpha > 0$, the stability condition corresponds to an overly rigid response of the contact surface deformation. The type of contact pressure distribution that develops in the case of partial contact $(\alpha < 0)$ is shown in Fig. 3. In that case, the contact pressure retains the singularity $(r^{-1/2})$ at the punch perimeter $(r = a)$ and drops to zero at the separation boundary $(r = a_s)$. This phenomenon may be particularly important in foundation engineering when the top soil may be overly compacted (and hence become much stiffer than the substrate), in combination with a rigid and largely spread footing (e.g., general foundation for tall buildings).

For the spherical punch of diameter D, the contact condition, $p(r) \geqslant 0$, requires

$$\frac{8\pi}{D} + \frac{P}{E_0}C_1\alpha^3 > 0, \tag{49a}$$

which predicts a critical load

$$\frac{P}{E_0 D^2} = -\frac{8\pi}{C_1}\frac{1}{(\alpha D)^3} = \frac{-0.062}{(\alpha D)^3} \quad (\alpha < 0). \tag{49b}$$

For loads above the critical value (49b), the contact condition $da\,dh \geqslant 0$ ($a = 0$ if and only if $h = 0$) is violated. As for the circular punch case, condition (49) becomes critical (loss of complete contact) only when $\alpha < 0$. The load-depth $(P-h)$ response is stable, if

$$\frac{P}{2\pi a E_0}\left\{\frac{\pi}{2} - \alpha^*\left(C_0 - \frac{C_1}{3}\alpha^{*2} + \frac{2}{45\pi}C_1^2\alpha^{*5}\right)\right\} + \frac{2}{3}\frac{a^2}{D}\left(1 - \frac{4}{15}C_1\alpha^{*3}\right) > 0. \tag{50}$$

The last condition predicts the critical loads

$$\frac{P}{E_0 D^2} = \frac{0.37}{(\alpha D)^3} \quad (\alpha > 0); \quad \frac{P}{E_0 D^2} = \frac{-0.24}{(\alpha D)^3} \quad (\alpha < 0).$$

Above these critical loads, the condition $\mathrm{d}h\,\mathrm{d}P > 0$ is not guaranteed by the present analysis. The normalized load, $P/(E_0 D^2)$ (often called "indentation stress"), is related to the normalized depth, h/D, and indirectly to the normalized contact radius, a/D (often called "indentation strain"). For $\alpha < 0$, the stability condition corresponds to an overall loss of stiffness in the spherical punch test. For $\alpha > 0$, the stability condition corresponds to an overly rigid response of the contact surface deformation.

Note that for punches other than flat, stability is intrinsically woven with the applied load, P. This is to be expected, if increasing the load, P, results in increasing the contact radius, a. Comparing (49) and (50), it can be shown that for $\alpha < 0$ complete contact is lost before unstable behavior commences, as was the case for the circular punch. For a soft-to-stiff elastic modulus gradation, the second derivative of its functional form with respect to depth plays an important role in the stability question: there is no stability (rigid response) problem for the power law case (concave functional), whereas there is stability problem for the exponential case, $\alpha > 0$ (convex functional).

Another interesting result is that for a conical indentor, no stability questions arise when,

$$1 - \frac{2C_1}{3\pi}\alpha^{*3} > 0. \tag{51}$$

This poses no restriction for $\alpha < 0$, but there are stability restrictions for $\alpha > 0$. This is plausible, because a sharp indentor stresses the surface more than the smooth indentor, hence a soft-to-stiff material ($\alpha > 0$) is more likely to be unstable at least for indentation depths comparable to the characteristic length $|\alpha^{-1}|$. On the other hand, apparently due to the severe penetration occurring near the cone tip, the cone will always be in contact with the body, in contrast to the circular flat and spherical punches.

These results suggest the following trends:

- The sharpness of the indentor, as expressed by the second derivative of the indentor profile, affects the contact and the stability condition of the exponential model as follows.
- Sharp indentors tend to have high critical loads where complete contact may be lost (e.g., cones and pyramids never lose complete contact).
- Sharp indentors tend to have stability problems only for stiff-to-soft gradation ($\alpha < 0$).
- Smooth indentors have stability problems for both stiff-to-soft ($\alpha < 0$) and soft-to-stiff ($\alpha > 0$) gradation, with partial loss of contact preceeding instability when $\alpha < 0$.
- For $\alpha < 0$, the stability condition corresponds to an overall loss of stiffness, whereas for $\alpha > 0$, the stability condition corresponds to an overly rigid response of the contact surface deformation.

There are some physical arguments which are appropriate to this juncture. Stability in the present context implies that an increase of load, P, leads to an increase of the indentation depth, h. From the present solutions, it is to be anticipated that for a smooth, convex indentor, the contact radius, a, increases with load. A compressive pressure is expected to act over the entire contact circular area in order to satisfy the duality of the contact unilateral condition with no adhesion (otherwise separation of the contacting surfaces may occur). The relative deformation that develops beneath the surface of the contact in the graded material is complicated and non-linearly related to the applied load. For certain material structures (depending on α), the load may be high enough to induce sub-surface deformation in such a way as to break the monotonicity of the contact radius-load ($a-P$) relation and subsequently of the load-depth ($P-h$) relation. It may argued on physical grounds that a material that becomes elastically softer with depth could give way to an indentor faster than the rate at which the load rises, since as the load increases, more

material beneath the surface is affected. This leads to separation (receding contact) of the indentor and the contacting surface, leading to multiple contact regions. The implication of such instability, if it happens, cannot be assessed analytically further. Possible sequential deformation scenarios depend also on the degree of plastification of the material. Dynamic effects cannot be excluded either, and a possible drop of load with increasing indentation depth should be considered in experiments and actual applications of the present contact analysis.

4. THE SPECIAL CASE OF A RIGID SPHERICAL INDENTOR

4.1. *The power law case*: $E = E_0 z^k$

In this case we approximate the *spherical* indentor with a parabolic indentor, hence $\beta = 2$ and $M = 1/D$ (where D is the diameter of the sphere), Fig. 4a. This approximation is valid for small contact radii, a; $a/D < 0.2$ in case of homogeneous solids (Yoffe, 1984), which cover all practical spherical indentations. The result for the contact pressure distribution can be readily obtained from eqn (41) as

$$p(r) = \frac{(3+k)P}{2\pi a^2}\left\{1 - \frac{r^2}{a^2}\right\}^{(1+k)/2}. \tag{52}$$

Obviously, the maximum contact pressure occurs at $r = 0$

$$p_{\max} = p(0) = \frac{(3+k)P}{2\pi a^2}. \tag{53}$$

The minimum contact pressure occurs at $r = a$ and $p_{\min} = p(a) = 0$. Note that, for a given load, P, the maximum pressure increases by a factor of $k/3$ relative to the maximum pressure in the corresponding homogeneous case ($k = 0$).

The depth-contact radius ($h-a$) relation for the spherical indentation of an elastic medium with a power-law variation of Young's modulus, reduces from eqn (39) to

$$h = \frac{a^2}{D}\frac{2}{k+1}. \tag{54}$$

The force-contact radius relation ($P-a$), eqn (40), becomes for the spherical case

$$a^{3+k} = PD\frac{c_1}{2^{2-k}\pi}\frac{(1+k)(3+k)}{2}\Gamma\left(\frac{1}{2}+\frac{k}{2}\right)\Gamma\left(\frac{3}{2}+\frac{k}{2}\right). \tag{55}$$

Combining eqns (54) and (55), we note the "size" effect in the force-depth relation, of the order $h^{k/2}$, which indicates that the indentation response stiffens with load, contrary to the homogeneous case where the elastic contact stiffness is constant. The force-depth response for the graded case is compared with the corresponding homogeneous case in Fig. 4b. Rostovtsev (1961) derived similar results (but incomplete in form) to eqns (54) and (55) by using another method which was based on the properties of polynomials as applied to contact problems.

Note that for the homogeneous case, $k = 0$, the solution precisely reduces to the classic Hertzian problem (Hertz, 1882):

$$h = 2\frac{a^2}{D}, \quad P\frac{1}{D^2} = \frac{E_0}{1-\nu^2}\frac{2\sqrt{2}}{3}\left(\frac{h}{D}\right)^{3/2}. \tag{56}$$

The vertical displacement outside the contact area ($a \leqslant r < \infty$) is

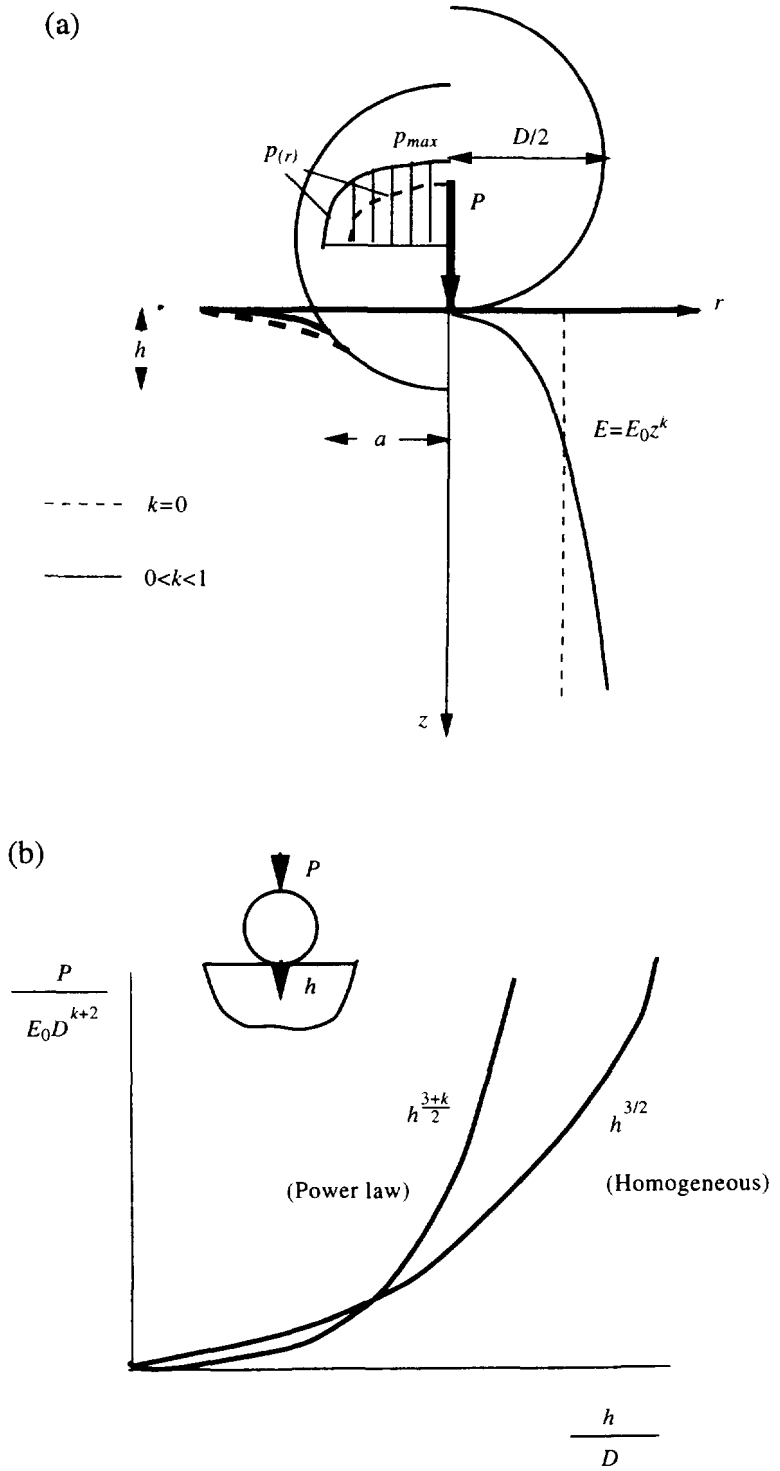

Fig. 4. (a) The spherical indentor problem for the power law case, $E = E_0z^k$. (b) The normalized force-depth $(P/(E_0D^{k+2}) - h/D)$ relation for the homogeneous and power law cases.

$$w(r) = \left\{\frac{a\sqrt{r^2-a^2}}{2} + \frac{1}{2}\left((r^2-2a^2)\arctan\left(\frac{a\sqrt{r^2-a^2}}{a^2-r^2}\right)\right)\right\} \times \frac{4\cos\frac{k\pi}{2}}{D\pi(1+k)}. \tag{57}$$

4.2. *The exponential law case*: $E = E_0e^{\alpha z}$

An approximate solution can be found for a *spherical* (parabolic) indentor of diameter D ($z_1 = r^2/D$), Fig. 5a. The pressure distribution, $p(r)$ $(0 \leqslant r \leqslant a)$, is

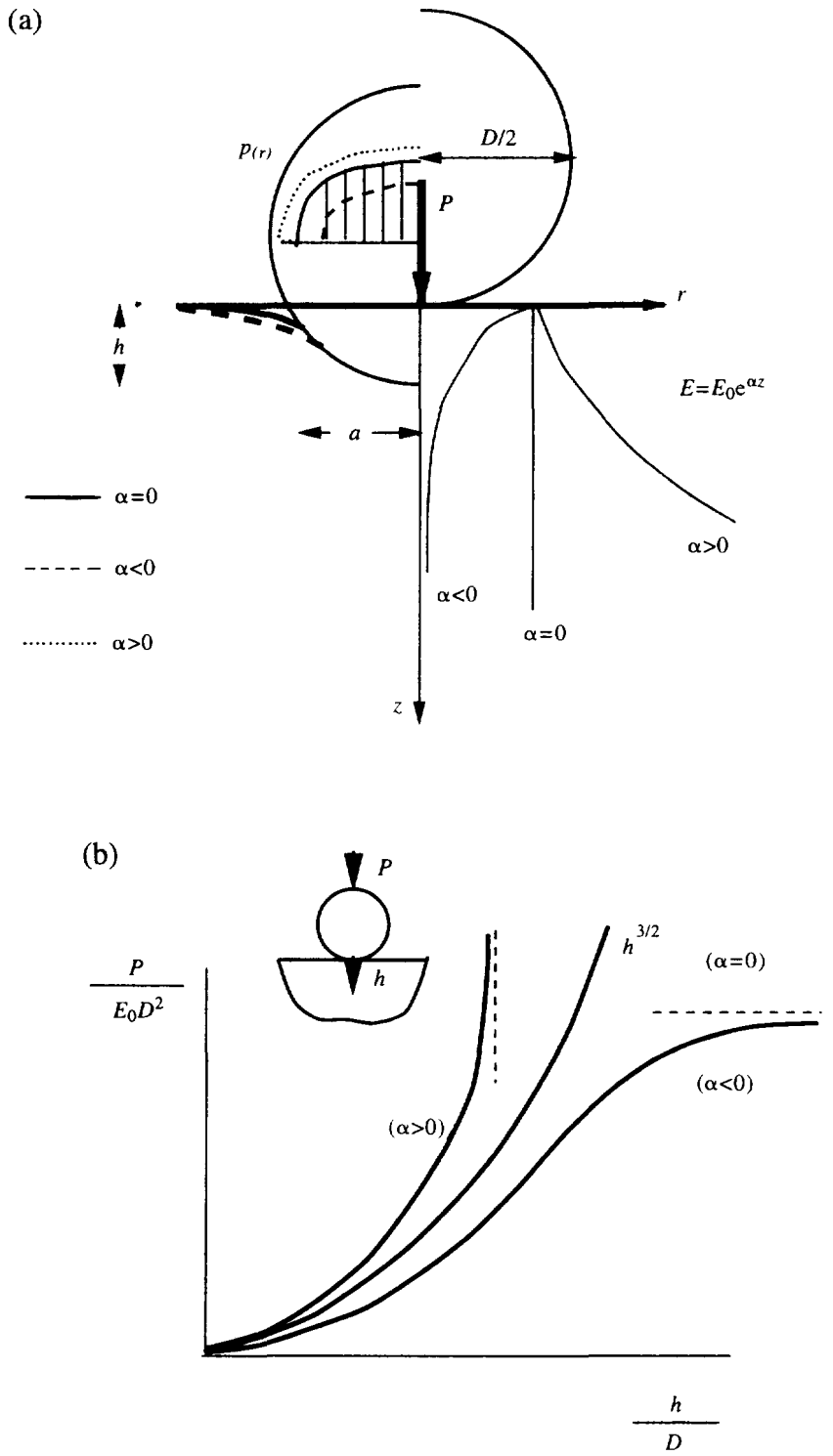

Fig. 5. (a) The spherical indentor problem for the exponential law case, $E = E_0 e^{\alpha z}$. (b) The normalized force-depth $(P/(E_0D^2) - h/D)$ relation for the homogeneous and exponential law cases.

$$p(r) \approx \frac{3P}{2\pi a^2}\left(1-\frac{r^2}{a^2}\right)^{1/2}, \tag{58}$$

which is the same as for the homogeneous case ($\alpha = 0$). The force-depth ($P-h$) relation is

$$h \approx \frac{P}{2\pi a E_0}\left\{\frac{\pi}{2} - \alpha^*\left(C_0 - \frac{C_1}{3}\alpha^{*2} + \frac{2}{45\pi}C_1^2\alpha^{*5}\right)\right\} + \frac{2}{3}\frac{a^2}{D}\left(1 - \frac{4}{15}C_1\alpha^{*3}\right). \tag{59}$$

The force-contact radius ($P-a$) relation is given by

$$a^3 \approx \frac{3\pi P}{E_0}\left(\frac{8\pi}{D} + \frac{P}{E_0}C_1\alpha^3\right)^{-1}. \tag{60}$$

Clearly, eqns (59) and (60) show a "size" effect in the form of decreasing stiffness with load, leading to a sigmoidal force-depth response for $\alpha < 0$ (completely below the homogeneous response) and an almost vertical (rigidly stiff) force-depth response for $\alpha > 0$ (completely above the homogeneous response), Fig. 5b.

5. THE SPECIAL CASE OF A RIGID CONICAL INDENTOR

5.1. *The power law case*: $E = E_0 z^k$

For the case of a *conical* indentor of semi-apical angle α, $\beta = 1$ and $M = \cot\alpha$, Fig. 6a. Then the pressure distribution is obtained from eqn (41), for the conical case to be

$$p(r) = \frac{P(1+k)(2+k)}{2\pi a^2}\int_{r/a}^{1}\left(t^2 - \frac{r^2}{a^2}\right)^{(k-1)/2} \mathrm{d}t. \tag{61}$$

For the homogeneous case, $k = 0$, eqn (61) reduces to the well known solution of Love (1939),

$$p(r) = \frac{P}{\pi a^2}\{-\ln(ar) + \ln[a^2 + a^2(\sqrt{1-(r/a)^2})]\} = \frac{E_0\cot\alpha}{2(1-\nu^2)}\operatorname{arccosh}(a/r), \tag{62}$$

which exhibits a logarithmic singularity at $r = 0$. For $k \neq 0$, the contact stresses have no singularity at $r = 0$ or at any other point of the surface. In fact, the finite value at $r = 0$ is the maximum contact pressure and is given by

$$p_{\max} = p(0) = \frac{P(1+k)(2+k)}{2\pi a^2 k}. \tag{63}$$

Note that $p_{\max} \to \infty$ for $k \to 0$. The lowest value of $p_{\max}$ ($= 3P/(\pi a^2)$) appears for $k \to 1$. The minimum contact pressure appears at $r = a$ and $p_{\min} = p(a) = 0$.

The depth-contact radius ($h-a$) relation reads as

$$h = a\frac{\sqrt{\pi}}{2\tan\alpha}\frac{\Gamma\left(\frac{1+k}{2}\right)}{\Gamma\left(1+\frac{k}{2}\right)}. \tag{64}$$

The contact radius, a, connects with the load, P, as (from eqn (40))

$$a^{2+k} = P\frac{c_1(1+k)(2+k)}{2^{1-k}\pi^{3/2}\cot\alpha}\Gamma\left(\frac{1+k}{2}\right)\Gamma\left(1+\frac{k}{2}\right). \tag{65}$$

Combining eqns (61) and (62), we note the "size" effect in the average pressure-depth relation, of the order h^k, which indicates that the average pressure (or hardness) increases with indentation depth. This is to be expected on the physical ground that a higher load

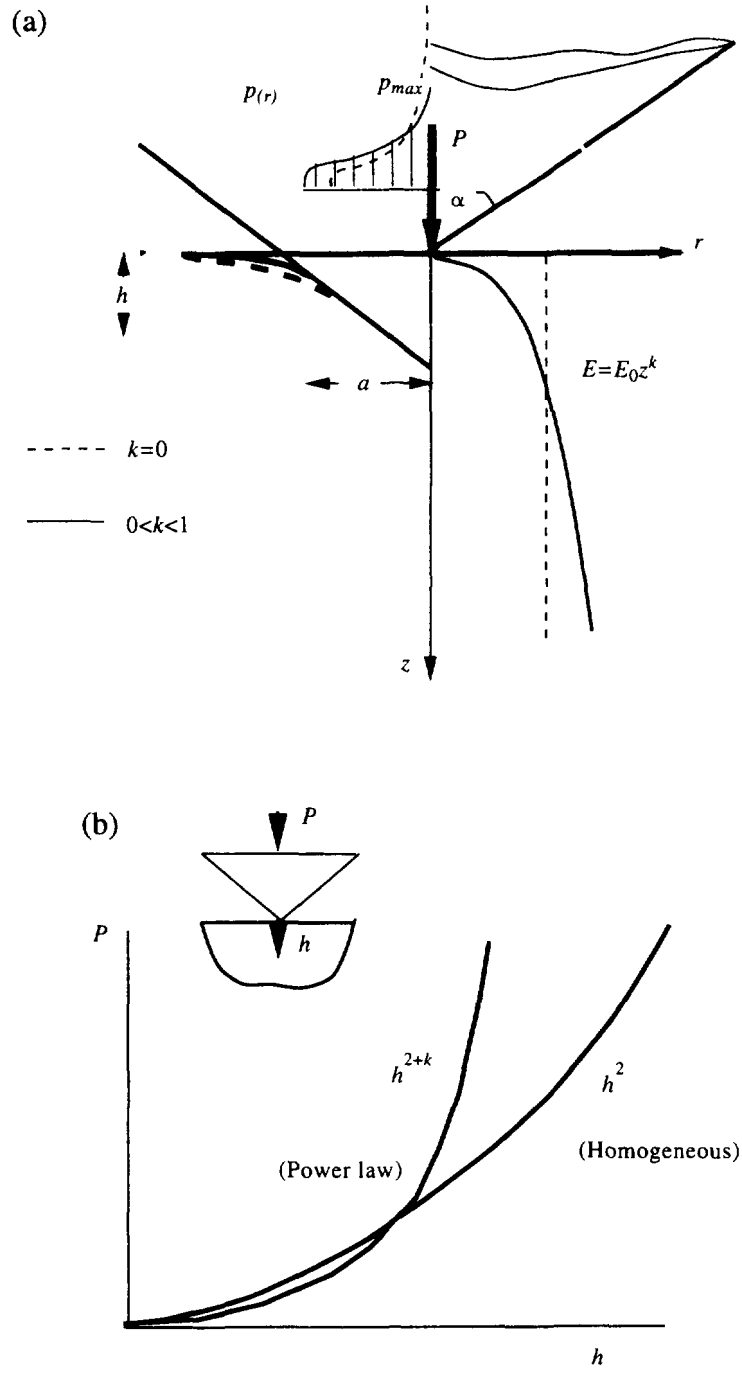

Fig. 6. (a) The conical indentor problem for the power law case, $E = E_0z^k$. (b) The normalized force-depth ($P-h$) relation for the homogeneous and power law cases.

affects a larger material volume beneath the surface which is stiffer than the surface material; this causes an overall stiffer contact behavior. In the homogeneous case, the average pressure-depth variation is constant, a fact that is used in hardness estimation as the average contact stress. Hence, elastic inhomogeneity at the surface may contribute to the experimentally observed "size" effect of sharp indentation tests. The force-depth response of a graded case is compared with the homogeneous case in Fig. 6b.

For the homogeneous case, $k = 0$, we retrieve Love's results

$$h = a\frac{\pi}{2\tan\alpha}, \quad P = a^2\frac{\pi}{2\tan\alpha}\frac{E_0}{1-\nu^2}. \tag{66}$$

The vertical deformation outside the contact area ($a \leqslant r < \infty$) is

$$w(r) = \left\{-r+\sqrt{r^2-a^2} - \arctan\left(\frac{a\sqrt{r^2-a^2}}{a^2-r^2}\right)\right\} \times \cot\alpha \frac{\cos\frac{k\pi}{2}}{\sqrt{\pi}} \frac{\Gamma\left(\frac{1+k}{2}\right)}{\Gamma\left(\frac{k}{2}+1\right)}. \tag{67}$$

5.2. *The exponential law case*: $E = E_0 e^{\alpha z}$

For a *conical* indentor of semi-apical angle γ ($z_1 = r\cot\gamma$), Fig. 5, the force-contact radius relation reads

$$P = 2\pi a\left(f_0 + \frac{4}{3\pi}C_1 f_1 \alpha^{*3}\right)\psi^{-1}, \tag{68}$$

where

$$f_0 = E_0\left(h - \frac{\pi}{4}a\cot\gamma\right), \quad f_1 = E_0\frac{\pi}{16}a\cot\gamma, \tag{69}$$

and C_1 and ψ are as defined before, eqn (59). The total force, P, is related to the contact area, a, as

$$P = \frac{\pi E_0 a^2}{2\left(1-\frac{2C_1}{3\pi}\alpha^{*3}\right)\tan\gamma}. \tag{70}$$

Using the geometric relation, $h = a\pi/(2\tan\gamma)$, which connects the contact radius, a, with the indentation depth, h, we can express (70) as a force-depth ($P-h$) relation. Clearly, the "size" effect appears since the force, P, is not a parabolic function of the depth, h, Fig. 7b. In all cases, at low values of h, the results are close to the homogeneous case. At high loads, a sigmoidal response appears for $\alpha < 0$, completely below the homogeneous response and a concave response for $\alpha > 0$, completely above the homogeneous case. In addition, it can be verified that the logarithmic singularity of the contact pressure distribution appears at the cone-tip ($r = 0$), as in the homogeneous case, eqn (62).

Note that for the homogeneous case, $\alpha = 0$ ($\alpha^* = 0$), we recover exactly the classical solutions for the circular punch, as well as for the spherical (eqn (56)) and the conical (eqn (66)) indentors (Harding and Sneddon, 1945).

6. FINITE ELEMENT RESULTS FOR THE RIGID CIRCULAR PUNCH

The foregoing analytical results provide closed-form solutions for the contact pressure distribution and surface displacements in the graded elastic medium loaded normally by an axisymmetric indentor. We now check these predictions with detailed finite element analyses. These computations provide additional information on the stress fields in the interior of the elastic solid. The numerical analysis is also capable of providing the effect of variation in ν as a function of z (not done here because of space restrictions, see Part I for further details).

The rigid indentors were loaded by displacement control, as is the case for indentation tests. The details of the finite element procedure and mesh have been discussed extensively

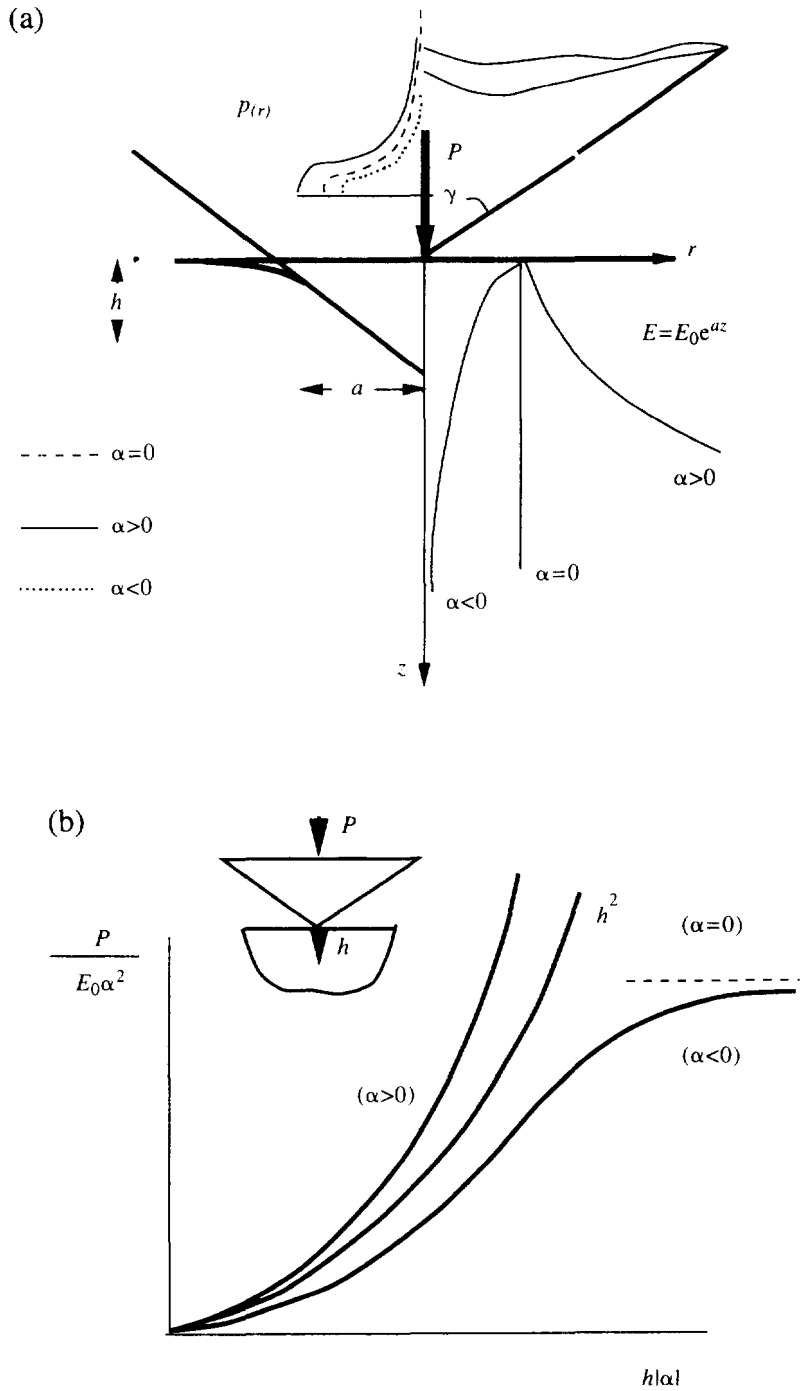

Fig. 7. (a) The conical indentor problem for the exponential law case, $E = E_0e^{\alpha z}$. (b) The normalized force-depth $(P/(E_0|\alpha|^2) - h|\alpha|)$ relation for the homogeneous and exponential law cases.

in Part I (Giannakopoulos and Suresh, 1997). A total of about 24 elements were allowed to come in contact in order to provide sufficient resolution in the computation of the fields around the indentors. The outer boundaries were taken to be at least 50 times the contact radius, to ensure semi-infinite conditions. In the present case, a rigid cylindrical punch of radius a (unit length) was pressed by a displacement of order $w_0/a = 0.005$ which was the same in order to make comparisons with the homogeneous case. In this paper we present only the fields for the circular flat punch case because of its generality and usefulness for all other axisymmetric punches. The finite element results for the spherical and cone

indentors for graded materials will be presented along with experiments in Suresh *et al.* (1996) and Alcala *et al.* (1996), respectively.

6.1. *The power law case*: $E = E_0 z^k$

A wide range of the parameter k ($k = 0.25, 0.5, 0.75, 1.0$) has been modeled. Several different values of Poisson ratio, v, below and above its critical value, $v_{cr} = 1/(k+2)$, were analysed. For a particular choice of w_0/a, the results are universal, if all lengths are normalized by the punch radius a, and the stresses by E_0. For each value of v and k, the normalized stress fields are completely determined in the normalized plane $(z/a, r/a)$ by the contours of constant in-plane normalized stresses $\sigma_{rr}/(E_0 a^k)$, $\sigma_{zz}/(E_0 a^k)$, $\sigma_{rz}/(E_0 a^k)$, and the circumferential stress $\sigma_{\theta\theta}/(E_0 a^k)$. It was proved that the Poisson ratio has a rather weak effect for the stress fields in the vicinity of the punch, because the singularity at the punch perimeter dominates the solution. Overall, higher Poisson ratios ($v \to 0.5$) resulted in a stiffer response, exactly as expected from the analysis. The computed values of the total force, P, and the contact pressure at the origin, $p(r = 0)$, were within 99% of the values predicted by the theory (eqns (5) and (7)). Of course, the singularity at the punch perimeter was not captured, since no special singular element was used. However, at a distance of one to two elements away from the contact perimeter, the computed solution was remarkably close to the theory.

For comparison, Fig. 8a shows the deformation of a homogeneous material, $k = 0$, with $v = 0.2$, under a circular punch. Figure 8b gives the isocontours of the normalized radial stresses σ_{rr}/E_0, Fig. 8c the normalized vertical stresses σ_{zz}/E_0, Fig. 8d the normalized shear stresses σ_{rz}/E_0 and Fig. 8e the normalized circumferential stresses $\sigma_{\theta\theta}/E_0$. Figure 9 contains all the corresponding fields relevant for a power law graded material, $k = 0.25$, with $v = 0.25$. It is obvious that for the same normalized indentation depth, w_0/a, less sinking-in develops for the power law case than for the homogeneous case, as expected from the analysis. The singularity at the contact perimeter is not as strong as for the homogeneous case, also expected from the analysis. The stress fields focus more in the

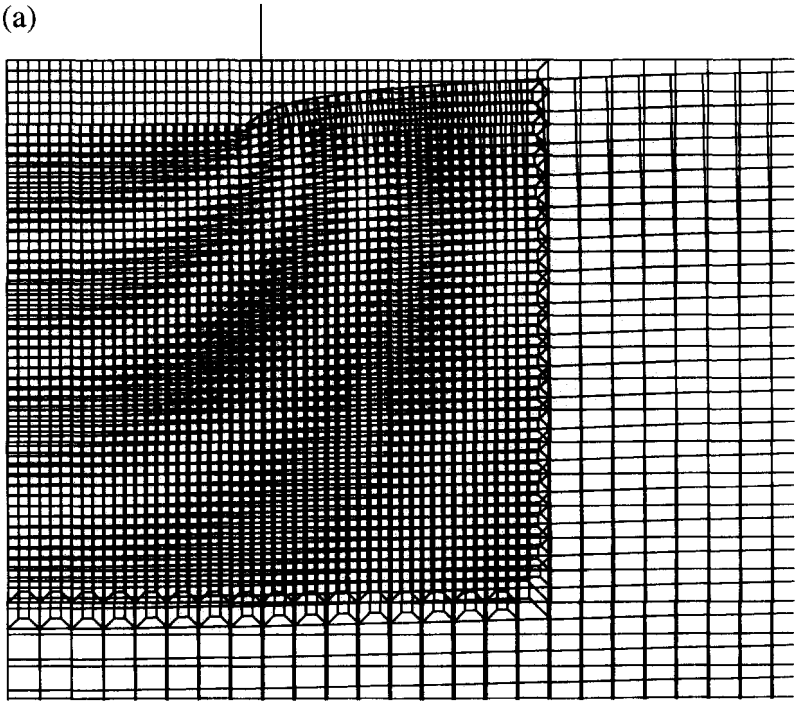

Fig. 8. (a) The deformation under a flat circular punch. Homogeneous case, $k = 0$, $v = 0.25$, $w_0/a = 0.005$. Displacements are magnified by 50. (b) Normalized radial stresses, $\sigma_{rr}/(E_0 a^k)$. (c) Normalized vertical stresses, $\sigma_{zz}/(E_0 a^k)$. (d) Normalized circumferential stresses, $\sigma_{\theta\theta}/(E_0 a^k)$. (e) Normalized shear stresses, $\sigma_{rz}/(E_0 a^k)$. (*Continued overleaf.*)

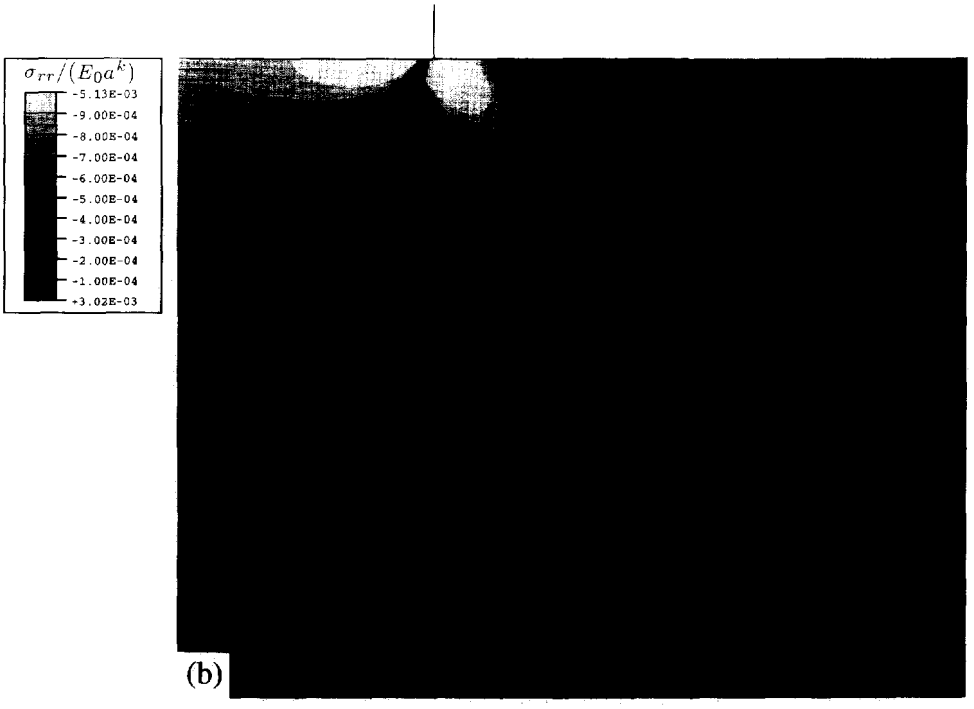

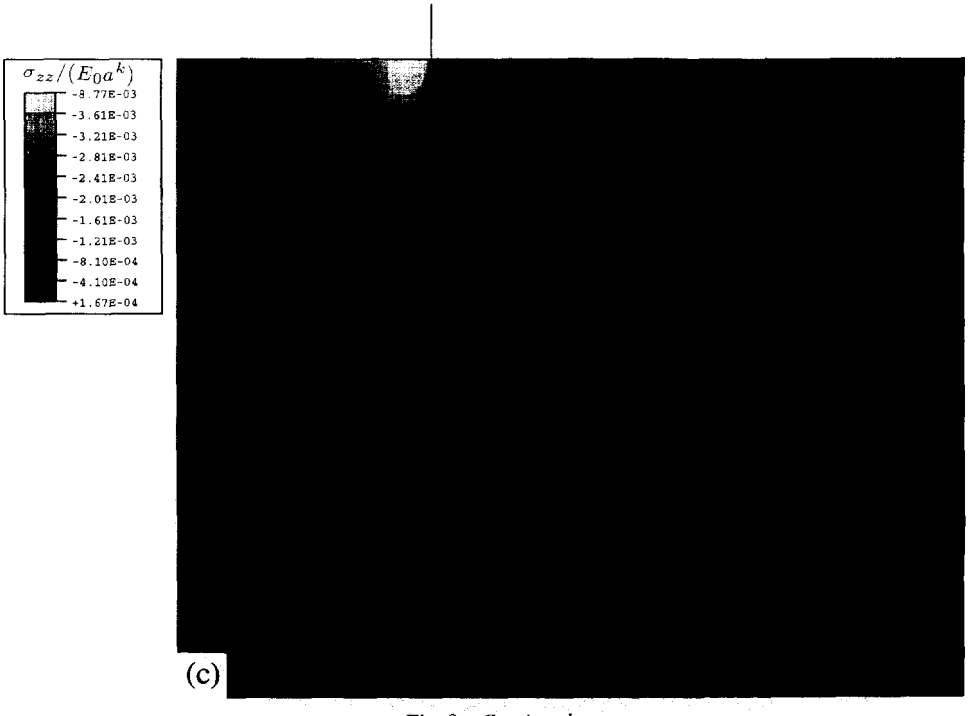

Fig. 8—*Continued.*

interior, indicating that possible plasticity or damage is expected to concentrate mainly in the interior rather that at the surface (compare Figs 8 and 9). The main results and comparisons for the flat punch on a material with power law elastic modulus distribution are summarized in Table 1. In all cases, the fields far away from the indented region conform to the point load solutions found in Part I (Giannakopoulos and Suresh, 1997), further confirming the validity of the present analysis and the robustness of the finite element methodology used in the context of the contact theory of graded materials.

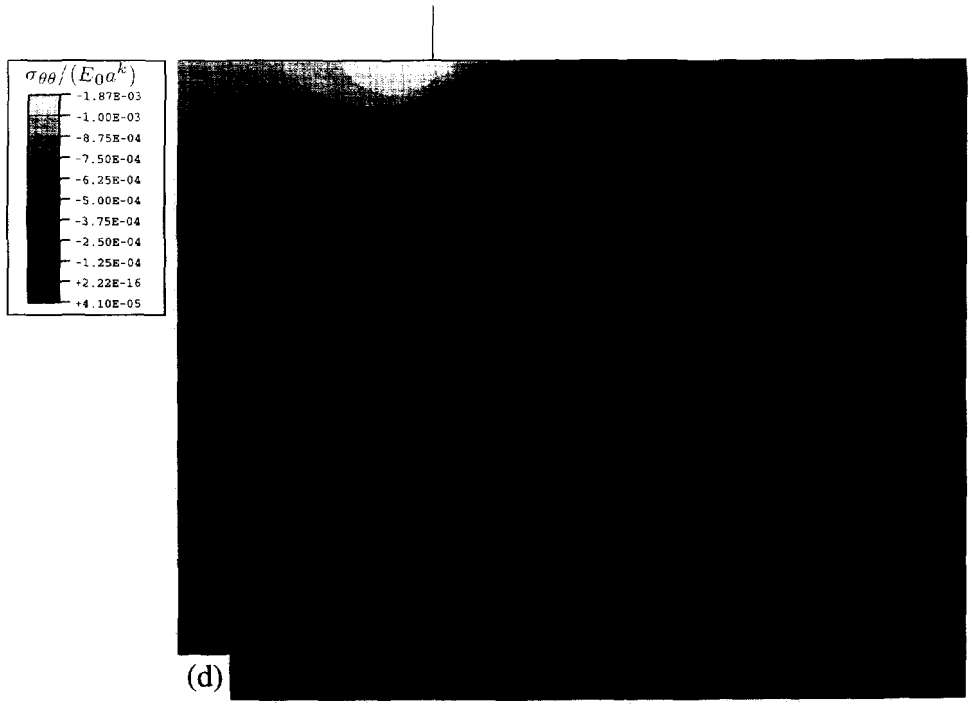

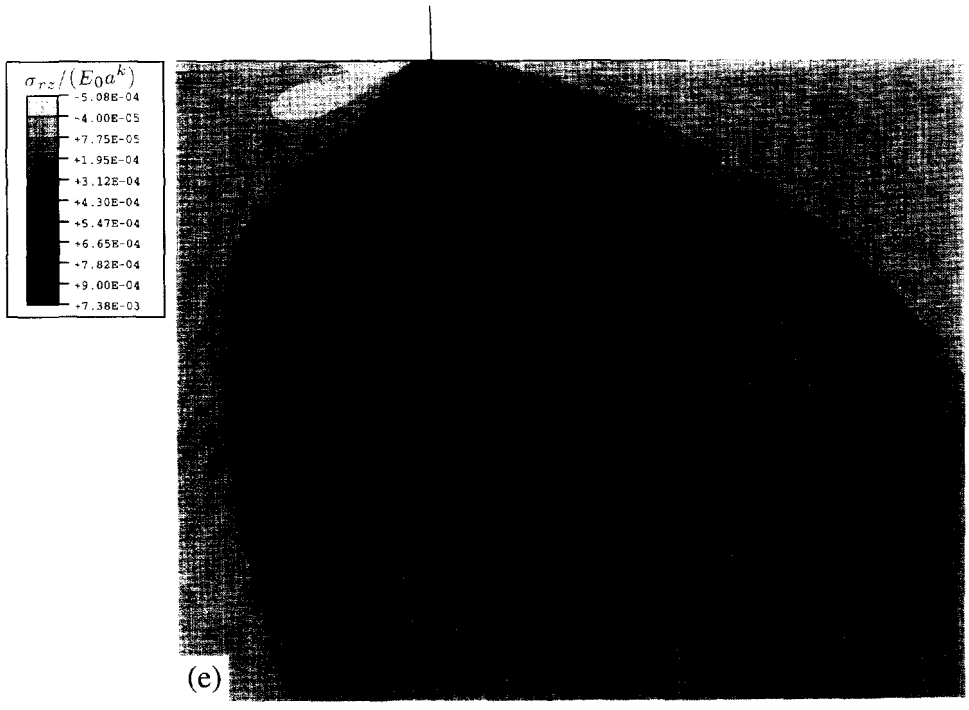

Fig. 8—*Continued.*

Table 1. Flat circular punch (power law model)

	Homogeneous (E_0)	Power law ($E_0 r^k$; $0 \leqslant k < 1$)
Force/depth correlation (P–h)	linear, increasing as $\nu \to 0.5$	linear, lower than the homogeneous case, increasing as $\nu \to 0.5$
Surface sinking-in	more than the inhomogeneous case	less than the homogeneous case
Singularity at the contact perimeter	$-1/2$	$(k-1)/2$
Contact conditions	complete contact	complete contact
Incremental stability	yes	yes
Stress fields close to the indentation	spread on the surface	focus in the interior

(a)

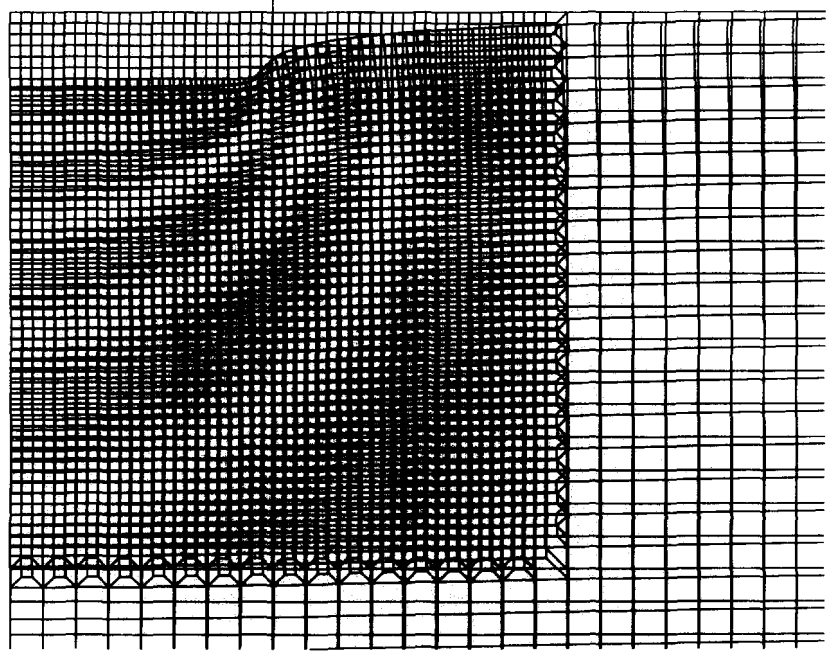

Fig. 9. (a) The deformation under a flat circular punch. Power law case, $k = 0.25$, $\nu = 0.25$, $w_0/a = 0.005$. Displacements are magnified by 50. (b) Normalized radial stresses, $\sigma_{rr}/(E_0 a^k)$. (c) Normalized vertical stresses, $\sigma_{zz}/(E_0 a^k)$. (d) Normalized circumferential stresses, $\sigma_{\theta\theta}/(E_0 a^k)$. (e) Normalized shear stresses, $\sigma_{rz}/(E_0 a^k)$. (*Continued opposite and overleaf.*)

6.2. *The exponential law case*: $E = E_0 e^{\alpha z}$

The exponential model was examined for a variety of positive and negative values of $\alpha^* = a\alpha$, with Poisson ratios, $\nu = 0$ and 0.3. The analytical results (eqns (33) and (34)) for the total force P and the contact pressure $p(r = 0)$ were less than 6% higher for $|\alpha^*| \leqslant 0.1$ when compared to the finite element results. They deviated more for increasing values of $|\alpha^*|$. This is expected, since the analytical results were obtained based on a two-term expansion around the value $\alpha^* = 0$. Nevertheless, all conclusions were qualitatively verified, but with the numerical values slightly higher than those predicted by the theoretical analysis.

For $\alpha < 0$, the normalized force, $P/P_{\alpha=0}$ ($P_{\alpha=0}$ is the force corresponding to the homogeneous case), drops precipitously from 1 to 0 (see Table 2). For $a\alpha \approx -1.125$, loss of complete contact is detected. The normalized separation radius, $\alpha_s\alpha$, increases from 0 to 1, as $a\alpha \leqslant 1.125$, until instability occurs at $a\alpha \approx -1.625$ (see Table 2). The sequence of these events (contact separation followed by instability) was correctly predicted by the theory (eqns (47) and (48)). For $\alpha > 0$, the normalized force, $P/P_{\alpha=0}$, increases slowly from 1 to 2 (see Table 2). For $a\alpha \approx 1$, instability occurs. No loss of complete contact is detected ($\alpha_s\alpha = 0$), as predicted by the theory. The Poisson ratio does not affect the above values much (see Table 2); however, it lowers the contact stiffness (indentation response is more compliant). This is contrary to the power law case where increasing the Poisson ratio results in higher contact stiffness.

Turning to the field variables, we plot three representative cases in Fig. 10 for $a\alpha = -0.2$, Fig. 11 for $a\alpha = -1.5$ (partial contact) and Fig. 12 for $a\alpha = 0.2$. Comparing Figs 8a, 10a and 12a, we observe that the amount of sinking-in of the surface is smaller for $\alpha > 0$ and large (extending well outside the contact regime) for $\alpha < 0$, compared to the homogeneous case ($\alpha = 0$). The stress fields in the vicinity of the contact area appear quite similar in shape with the homogeneous case (Fig. 8), with the exception of the case of partial contact (Fig. 11). However, the stress magnitudes are much stronger for $\alpha > 0$ and weaker for $\alpha < 0$. This is expected, since the stresses have a square-root singularity which

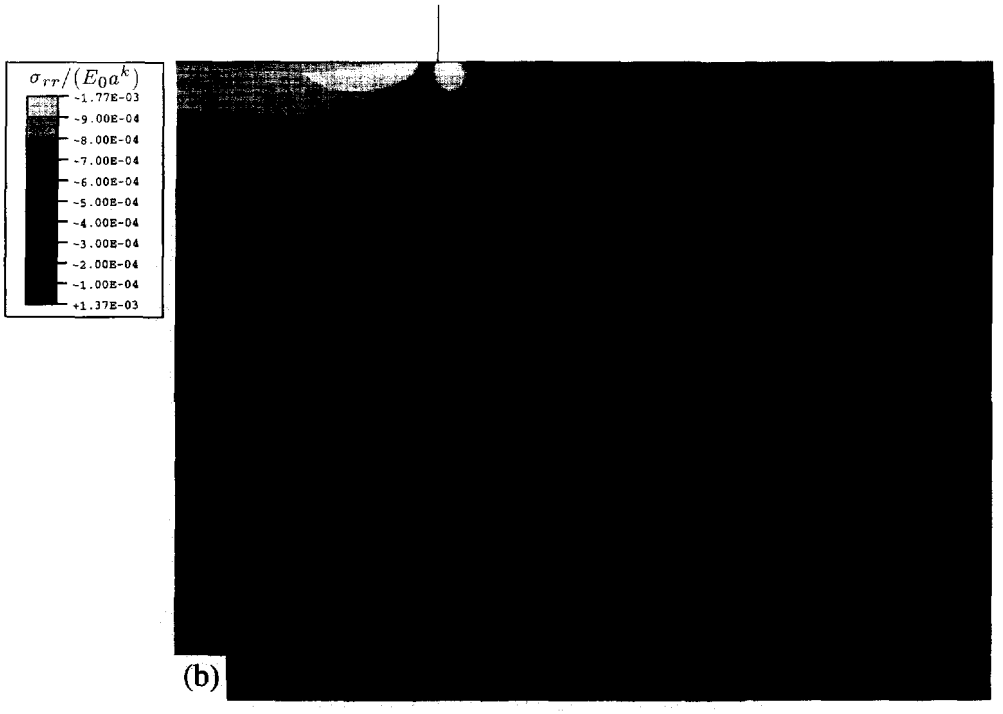

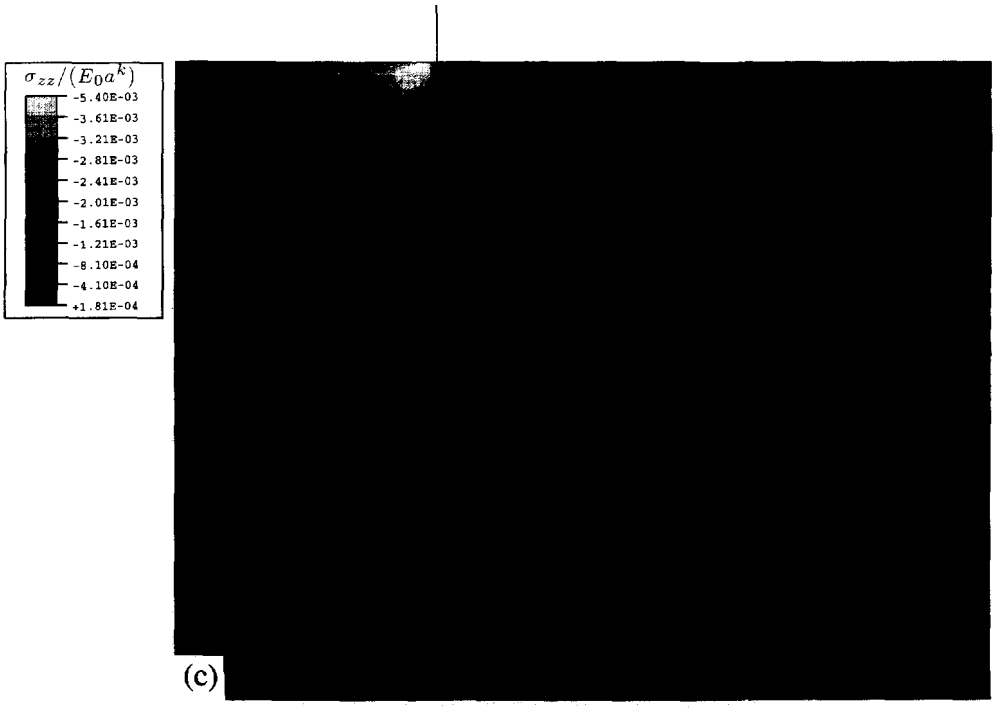

Fig. 9—*Continued.*

dominates the fields in the vicinity of the contact area. The comparisons of the overall response of the exponential case with the homogeneous case are summarized in Table 3. In all cases, the fields far away from the indented region converge to the point load solutions found in Part I (Giannakopoulos and Suresh, 1997), further confirming the validity of the present analysis and the robustness of the finite elements used for the indentation of graded materials. Obviously, other types of rigid or elastic indentors, as well as other elastic gradations of elastic properties, could be easily analyzed with the present finite element formulation.

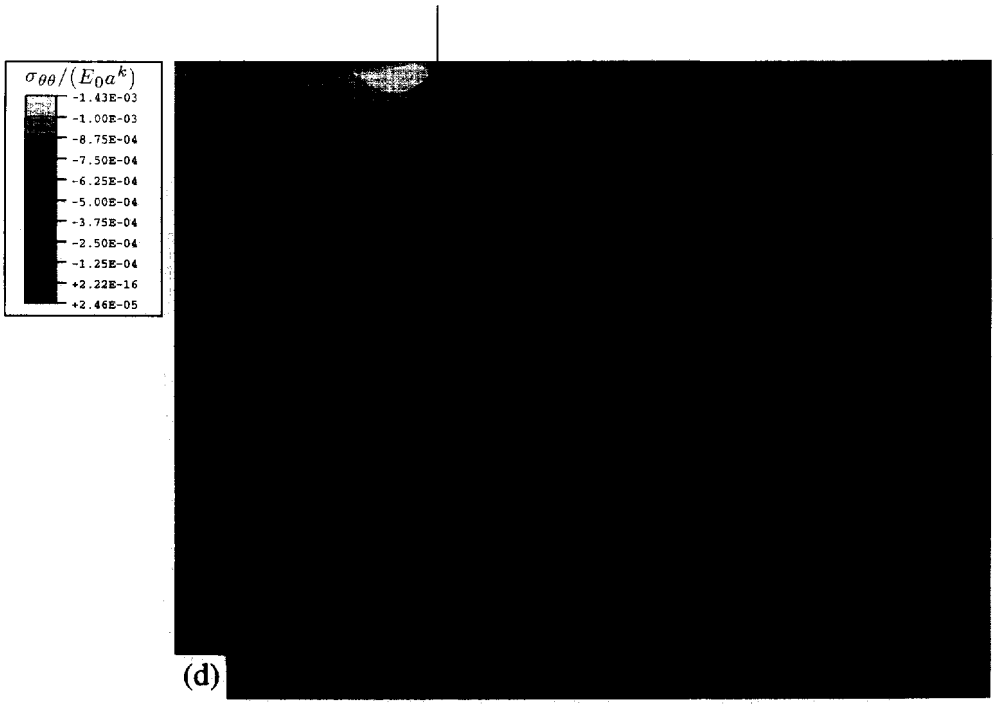

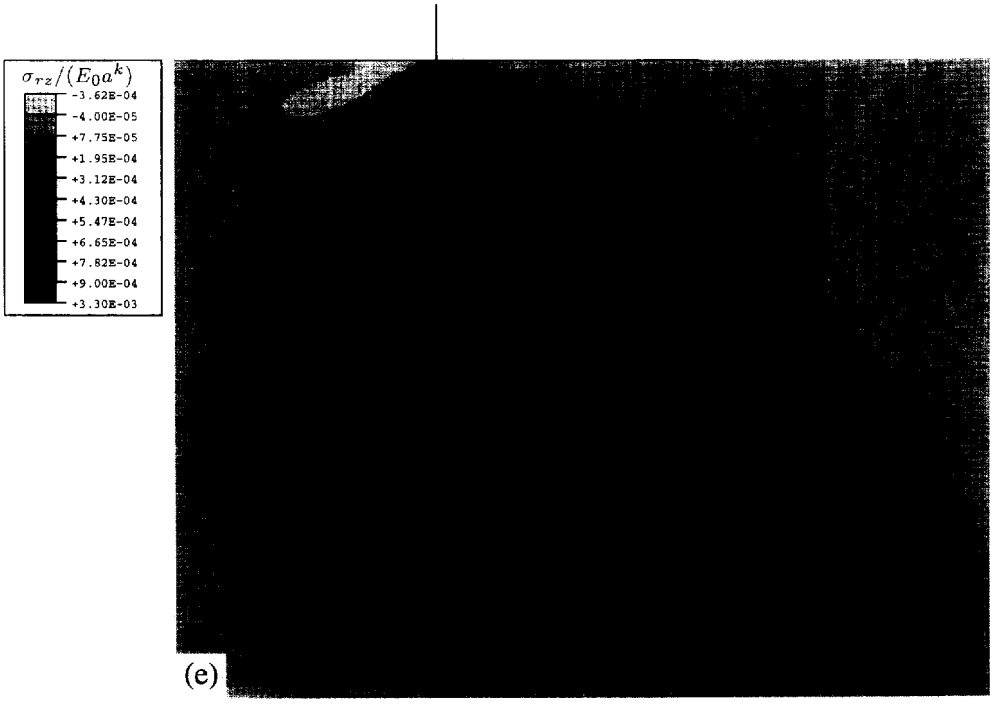

Fig. 9—*Continued.*

7. CONCLUSIONS

The present paper examines the indentation of solids with gradients in elastic properties with axisymmetric indentors. Two main elastic gradiation functions with depth, z, were examined: the power ($E = E_0 z^k$) and the exponential ($E = E_0 e^{\alpha z}$) law. These are representative cases of many types of materials in mechanical and geotechnical applications. Three kinds of rigid, frictionless indentors were examined: the circular flat punch, the spherical and the conical punch. Such indentors are of particular interest in foundation

Table 2. Finite element results for the exponential model (flat circular punch). Load, P, normalized by the corresponding homogeneous case, $P_{\alpha=0}$, for the same indentation depth. Corresponding fraction of the separation radius (a_s/a)

$\alpha^* = \alpha a$	$P/P_\alpha = 0$ $\nu = 0.0$	$P/P_\alpha = 0$ $\nu = 0.3$	a_s/a $\nu = 0.0, 0.3$
0.00	1.000	1.000	0.00
−0.05	0.862	0.767	0.00
−0.10	0.545	0.489	0.00
−0.15	0.288	0.280	0.00
−0.20	0.155	0.160	0.00
−0.25	0.089	0.096	0.00
−0.50	0.0123	0.0141	0.00
−1.00	0.00133	0.00170	0.00
−1.225	0.00089	0.00102	0.25
−1.25	0.00062	0.00070	0.50
−1.50	0.000033	0.000037	0.67
−1.625	Instability	Instability	—
0.00	1.000	1.000	0.00
0.05	1.179	1.097	0.00
0.10	1.277	1.198	0.00
0.15	1.365	1.280	0.00
0.20	1.448	1.377	0.00
0.25	1.528	1.461	0.00
0.50	1.900	1.862	0.00
1.00	Instability	Instability	0.00

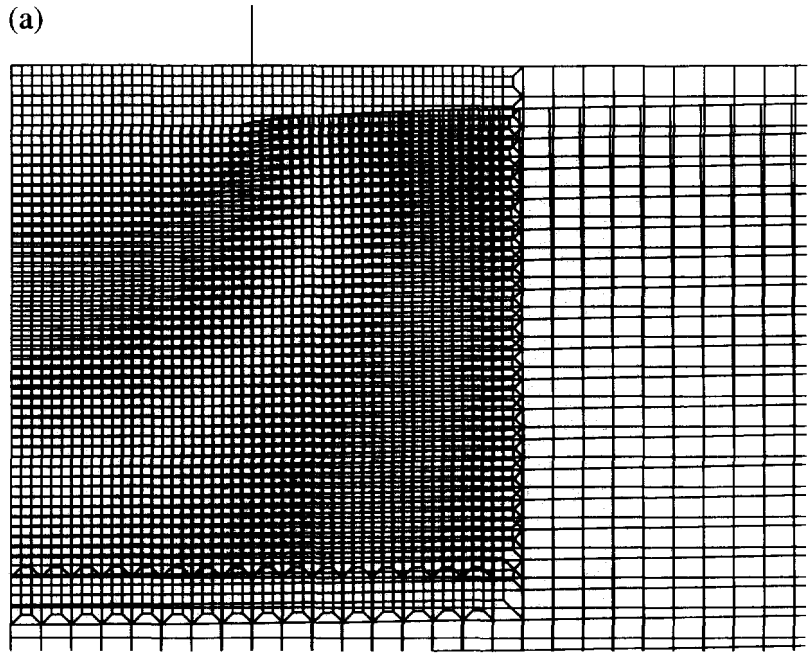

Fig. 10. (a) The deformation under a flat circular punch. Exponential law case, $a\alpha = -0.2$, $\nu = 0.2$, $w_0/a = 0.005$. Displacements are magnified by 50. (b) Normalized radial stresses, σ_{rr}/E_0. (c) Normalized vertical stresses, σ_{zz}/E_0. (d) Normalized circumferential stresses, $\sigma_{\theta\theta}/E_0$. (e) Normalized shear stresses, σ_{rz}/E_0. (*Continued overleaf.*)

engineering as well as in indentation testing of inhomogeneous materials with smooth or sharp indentors.

The theoretical analysis was based on the results for the point force acting normally to the surface of a semi-infinite space which is locally isotropic with constant Poisson ratio (Giannakopoulos and Suresh, 1997; Part I). The circular flat punch was then examined and the attendant results used to construct corresponding solutions for the spherical and conical punch, as well as for any convex axisymmetric indentor. From the theoretical

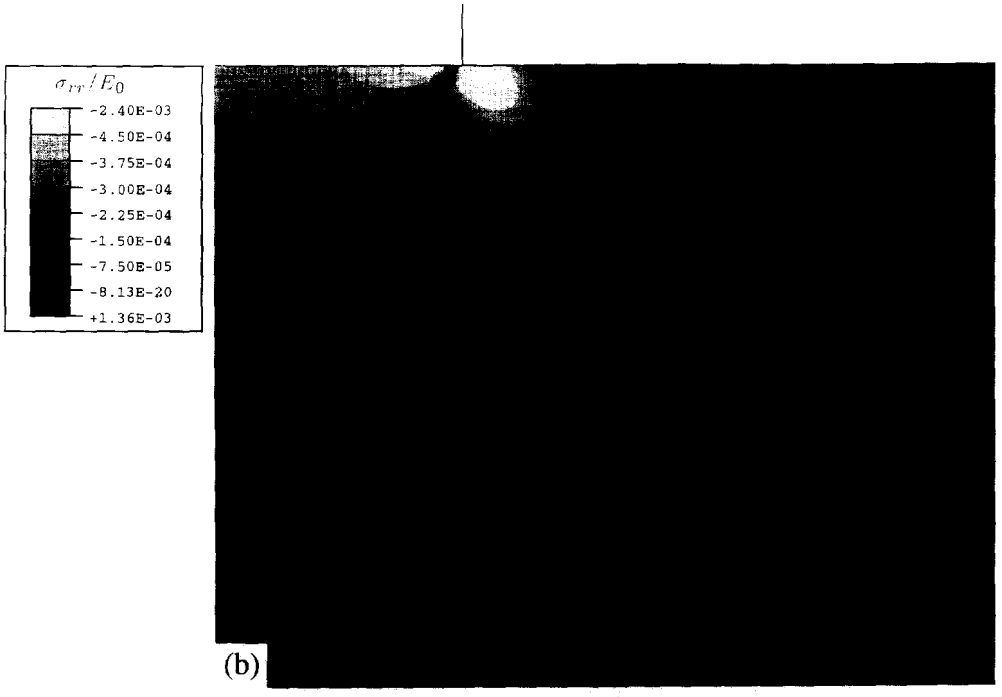

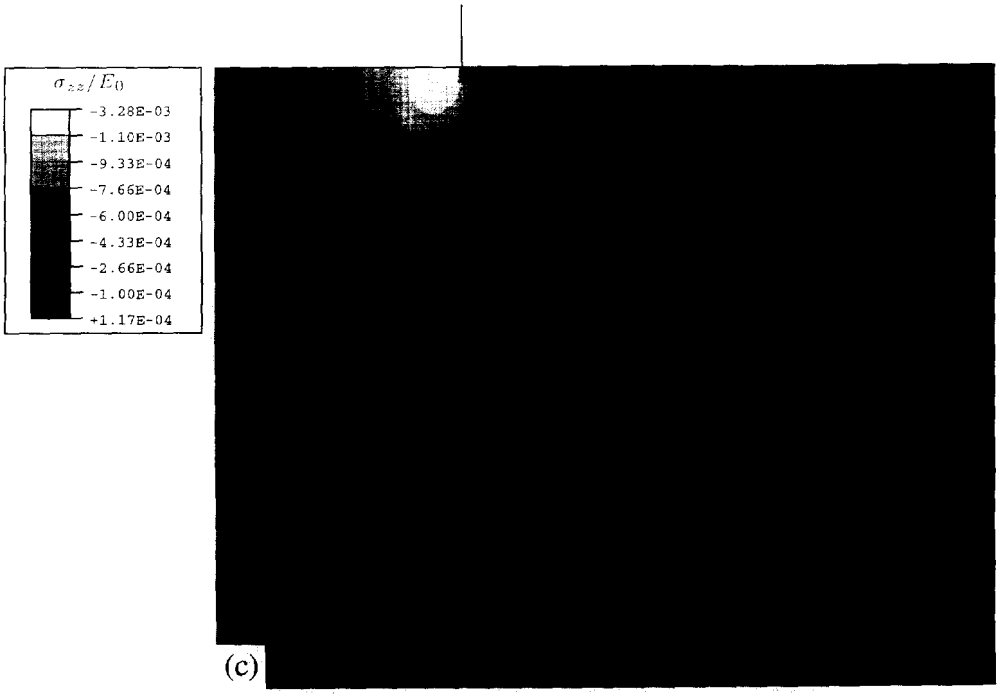

Fig. 10—*Continued.*

analysis, it was possible to obtain in closed form results such as the force-depth relations, the depth-contact radius relations and the contact pressure distributions. Subsequently, full finite element solutions were employed to confirm all the theoretical results, thus proving the robustness of the theory. In the present paper, we show only the finite element results for the circular flat punch problem. The main conclusions of this work are as follows.

(1) A soft-to-stiff elastic gradient beneath the surface does not always represent a soft contact response. The power law model and the exponential law model (for $\alpha > 0$) indicate soft and stiff contact responses, respectively.

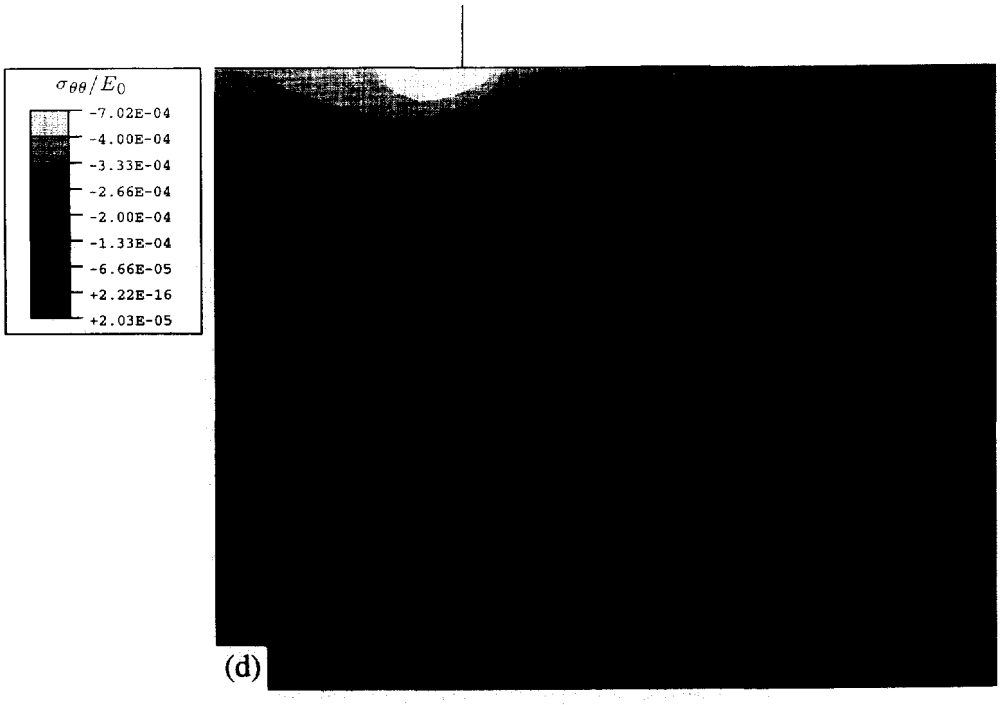

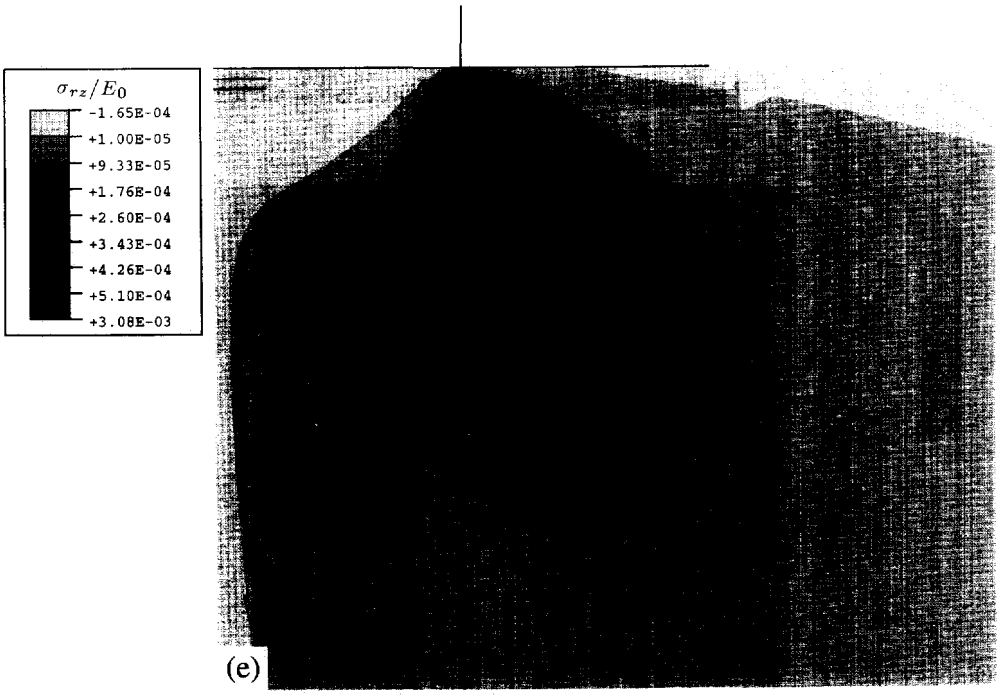

Fig. 10—*Continued.*

(2) The stiff-to-soft elastic gradient may lead to a complete loss of contact in case of smooth indentors. The stiff-to-soft gradient could lead to stability problems for sufficiently high applied force or contact radius. A rapidly varying soft-to-stiff elastic gradient may also lead to stability problems for sufficiently high loads.

(3) The milder contact pressure singularity at the perimeter of a flat punch and the absence of contact pressure singularity at the cone-tip in the power law case are noted.

(4) An increase in the Poisson ratio stiffens the contact response for the power law case and softens the contact response for the exponential law case. The Poisson ratio has little influence on the stress fields of the flat punch and the conical indentors, due to the stress concentration developed in the vicinity of the contact area.

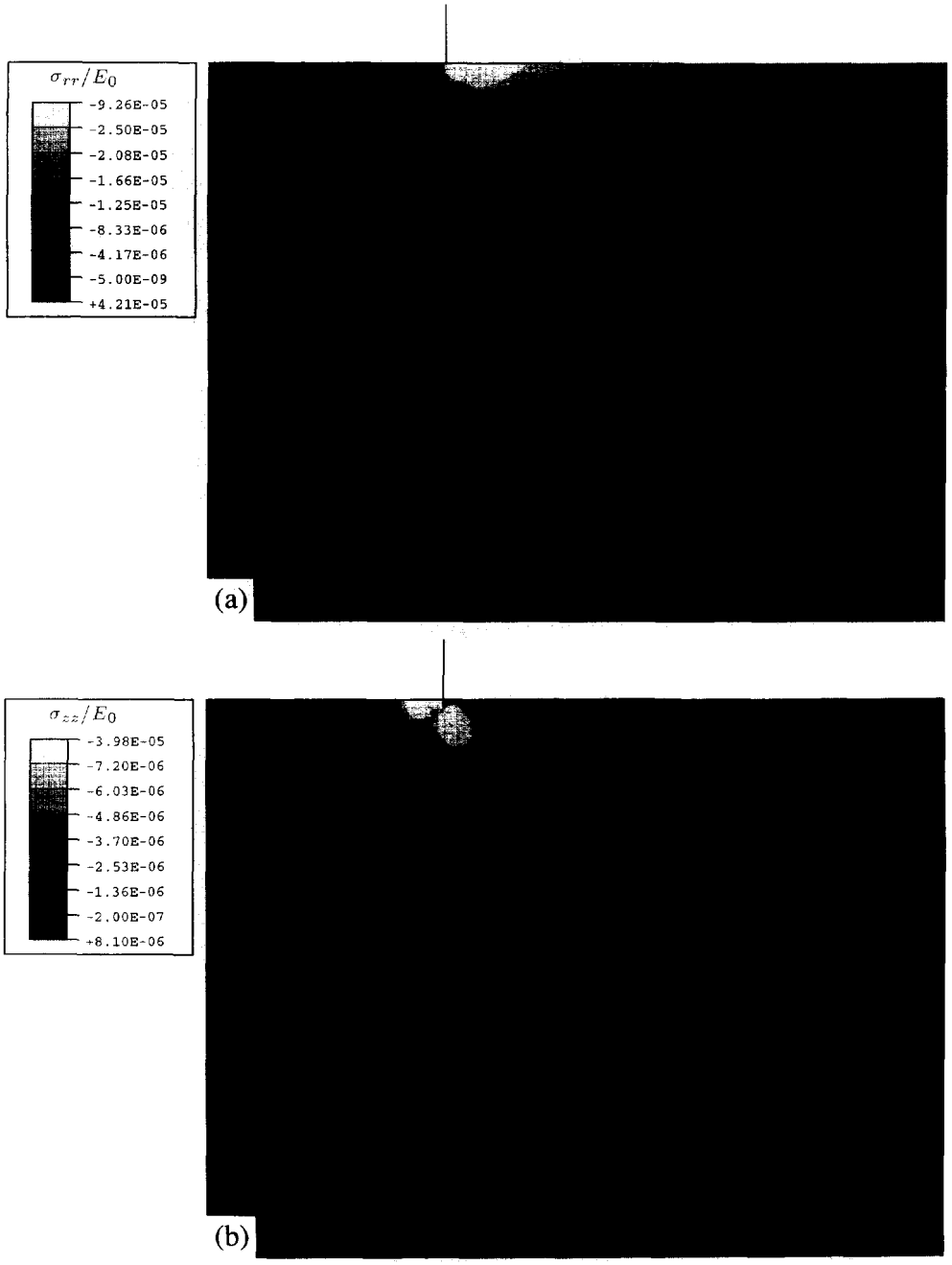

Fig. 11. The flat circular punch. Exponential law case, $a\alpha = -1.5$, $\nu = 0.2$, $w_0/a = 0.005$. Displacements are magnified by 50. Partial contact develops in the center of the contact. (a) Normalized radial stresses, σ_{rr}/E_0. (b) Normalized vertical stresses, σ_{zz}/E_0. (c) Normalized circumferential stresses, $\sigma_{\theta\theta}/E_0$. (d) Normalized shear stresses, σ_{rz}/E_0. (*Continued opposite.*)

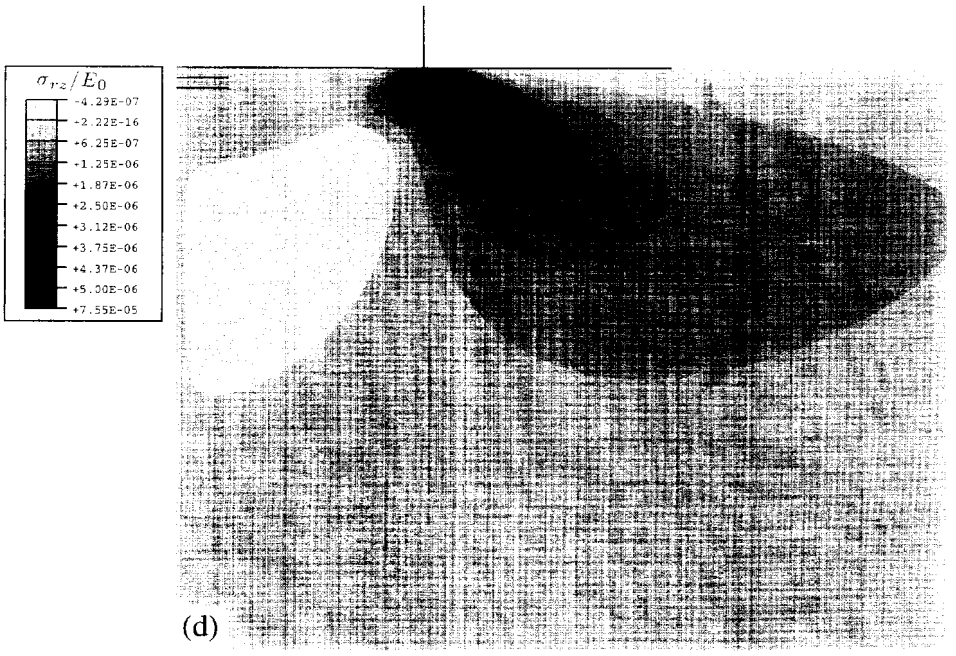

Fig. 11—*Continued.*

Table 3. Flat circular punch (exponential law)

	Homogeneous (E_0) $\alpha = 0$	Exponential ($Ee^{\alpha z}$) $\alpha < 0$	$\alpha > 0$
Force/depth correlation (P–h)	linear, increasing as $\nu \to 0.5$	linear, lower than the homogeneous case, decreasing as $\nu \to 0.5$	linear, higher than the homogeneous case, decreasing as $\nu \to 0.5$
Surface sinking-in		more than the homogeneous case, extends considerably at the surface	less than the homogeneous case
Singularity at the contact perimeter	$-1/2$	-1.2	-1.2
Contact conditions	complete contact	loss of contact at $\alpha a = -1.225$	complete contact
Incremental stability	yes	loss of stability at $\alpha a = -1.625$	loss of stability at $\alpha a = 1.000$
Stress fields close to the indenter	spread at the surface	similar to but weaker than the homogeneous case, considerably different when loss of contact occurs	similar to but stronger than the homogeneous case

(5) In all cases, the "size" effect, as exemplified in the estimation of the average contact pressure was evident. This quantitatively indicates the influence of the elastic inhomogeneity on the hardness calculations. The conical punch results imply in particular an increasing hardness for a soft-to-stiff response and a decreasing hardness for a stiff-to-soft response.

(6) For the power law case, the Poisson ratio has important implications for the spherical punch problem. A Poisson ratio lower than the critical value, $1/(k+2)$, resulted in moving the point of maximum Mises stress closer to the surface. On the other hand, a Poisson ratio higher than $1/(k+2)$ resulted in eliminating the tensile in-plane principal stresses responsible for the Hertzian type of cracking.

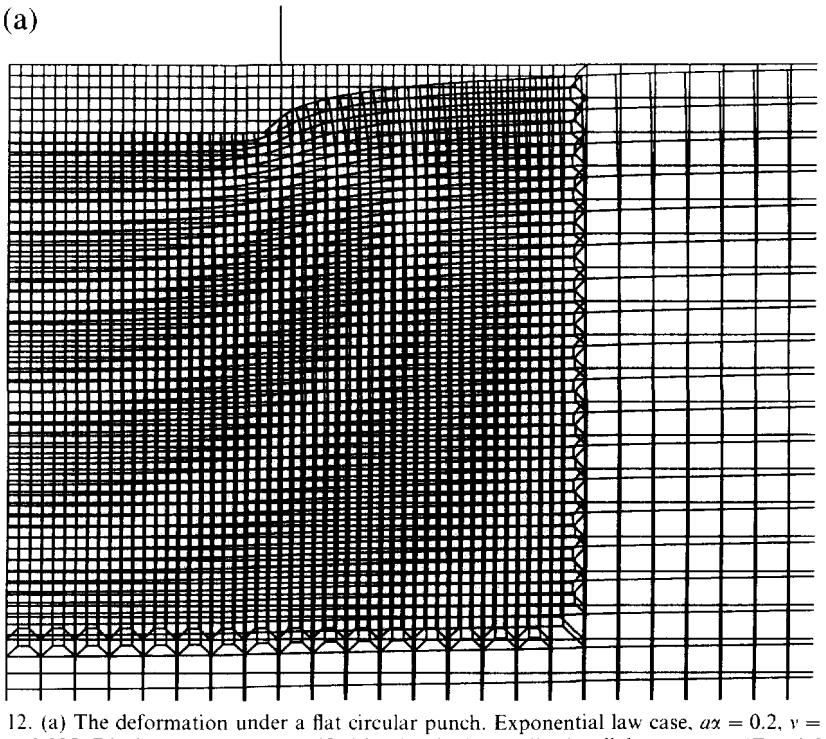

Fig. 12. (a) The deformation under a flat circular punch. Exponential law case, $a\alpha = 0.2$, $\nu = 0.2$, $w_0/a = 0.005$. Displacements are magnified by 50. (b) Normalized radial stresses, σ_{rr}/E_0. (c) Normalized vertical stresses, σ_{zz}/E_0. (d) Normalized circumferential stresses, $\sigma_{\theta\theta}/E_0$. (e) Normalized shear stresses, σ_{rz}/E_0. (*Continued opposite and overleaf.*)

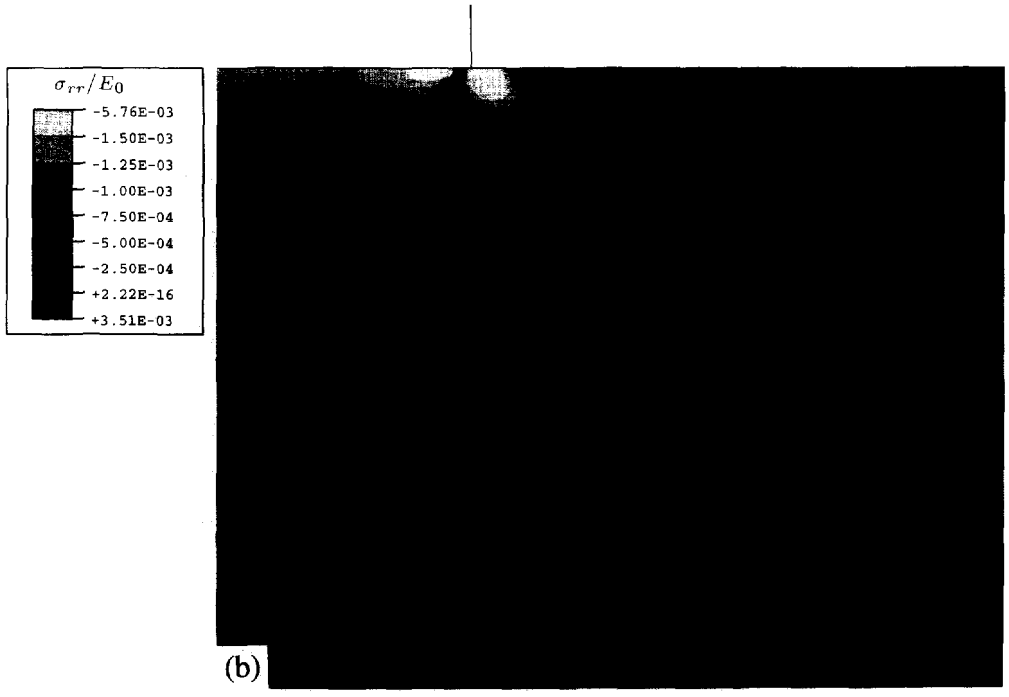

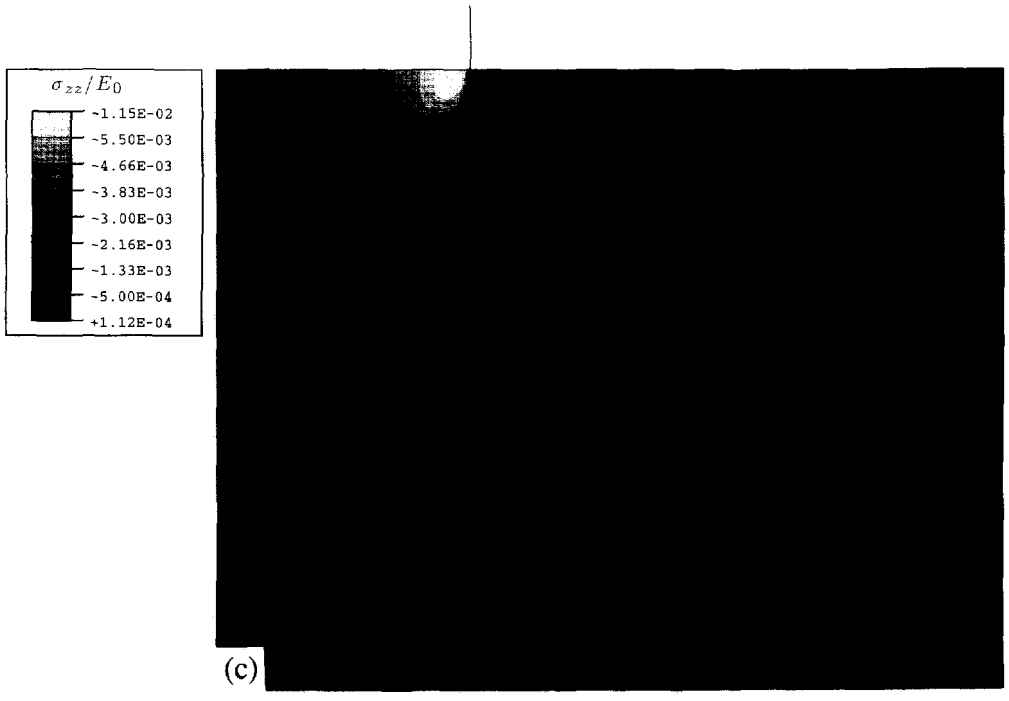

Fig. 12—*Continued.*

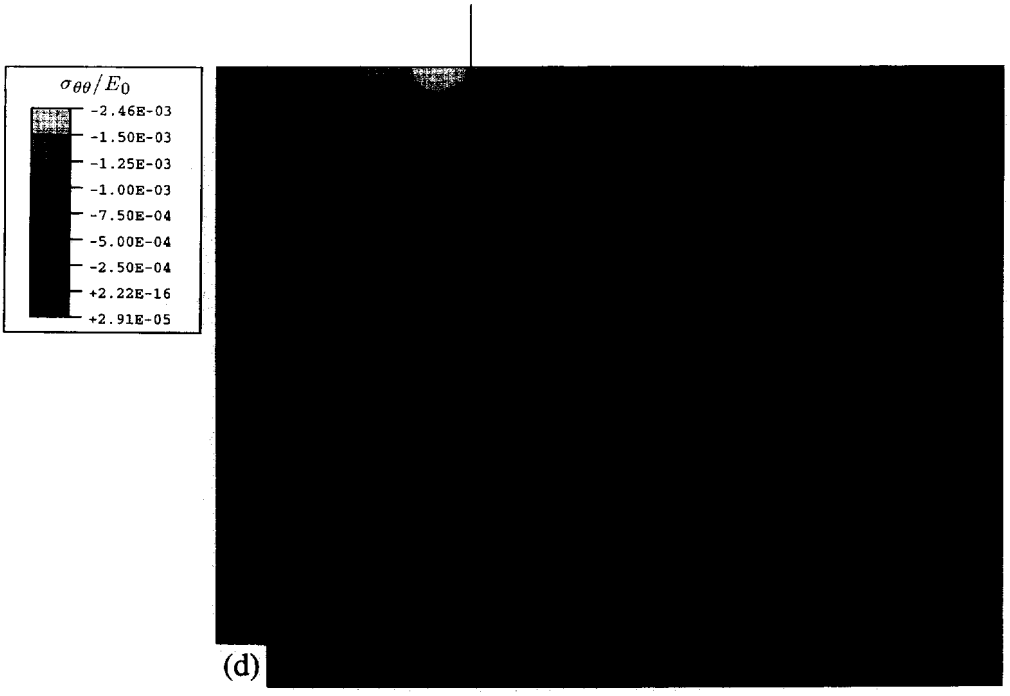

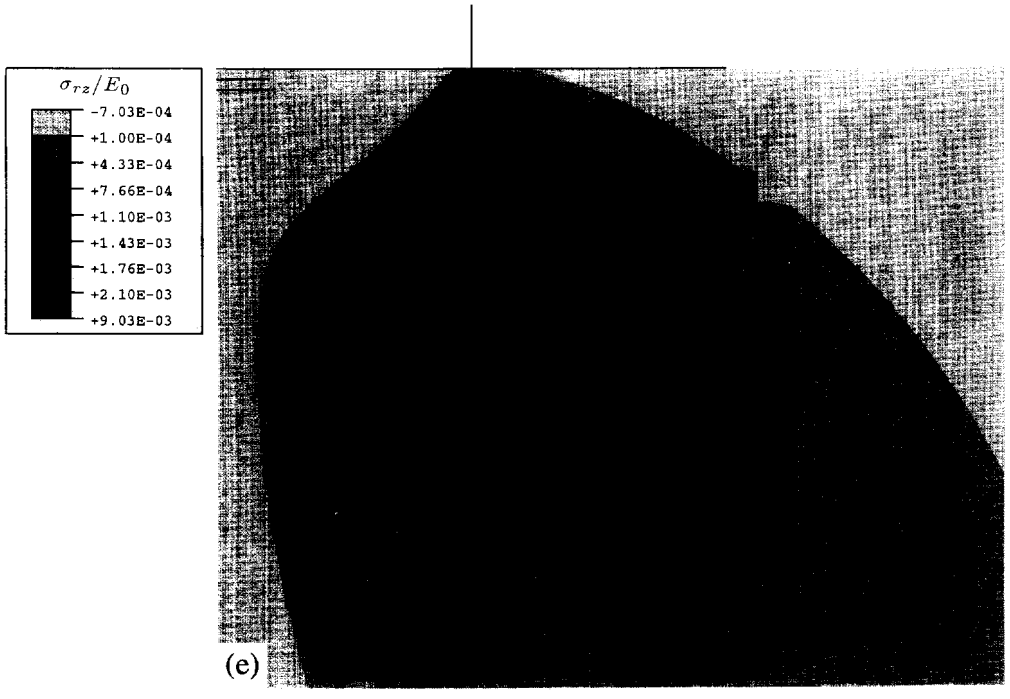

Fig. 12—*Continued.*

(7) The stress fields for the power law case are focused more in the interior than the corresponding homogeneous or the exponential case, indicating that possible development of plasticity and/or damage will be confined in the interior below the contact region. The reverse is true for the power law case ($\alpha < 0$).

Acknowledgements—This work has been supported by the U.S. Office of Naval Research under Grant N00014-94-1-0139 to MIT.

REFERENCES

Alcala, J., Giannakopoulos, A. E. and Suresh, S. (1996). Sharp indentation of solids with gradients in elastic properties. Work in progress.

Booker, J. R., Balaam, N. P. and Davis, E. H. (1985). The behaviour of an elastic non-homogeneous half-space. Part II—Circular and strip footings. *International Journal of Numerical and Analytical Methods in Geomechanics* **9,** 369–381.

Busbridge, I. W. (1938). Dual integral equations. In *Proceedings of the London Mathematical Society*, Second Series, vol. 44, pp. 115–129.

Fabrikant, V. I. (1989). *Application of Potential Theory in Mechanics*, Kluer Academic Publ., Dordrecht, Netherlands.

Calladine, X. and Greenwood, J. A. (1978). Line and point loads on a non-homogeneous incompressible elastic half-space. *Quarterly Journal of Mechanics and Applied Mathematics* **31,** 507–529.

Giannakopoulos, A. E. and Suresh, S. (1997). Indentation of solids with gradients in elastic properties: Part I. Point force. *Internationl Journal of Solids and Structures* **34,** 2357–2392.

Gibson, R. E. (1967). Some results concerning displacements and stresses in a non-homogeneous elastic half-space. *Geotechnique* **17,** 58–67.

Gibson, R. E. and Kalsi, G. S. (1974). The surface settlement of a linearly inhomogeneous cross-anisotropic elastic half-space. *ZAMP* **25,** 843–847.

Harding, J. W. and Sneddon, I. N. (1945). The elastic stresses produced by indentation of the plane surface of a semi-infinite elastic solid by a rigid punch. In *Proceedings of Cambridge Philosophical Society* **41,** 16–26.

Hertz, H. (1882). Uber die beruhrung fester elastischer koper. *Journal reine angewandte Mathematik* **92,** 156–171.

Hill, R. and Storakers, B. (1990). A concise treatment of axisymmetric indentation in elasticity. In *Elasticity: Mathematical Methods and Applications* (eds G. Eason and R. W. Ogden), Ellis Horwood Ltd., pp. 199–209.

Hruban, K. (1958). The basic problem of a non-linear and non-homogeneous half-space. In *Non-homogeneity in Elasticity and Plasticity IUTAM Symposium*, Warsaw, Pergamon Press, pp. 53–61.

Kassir, M. K. (1972). Boussinesq problems for non-homogeneous materials. *ASCE Journal of Engineering Mechanics Division* **98,** 457–470.

Love, A. E. (1939). Boussinesq's problem for a rigid cone. *Quarterly Journal of Mathematics* **10,** 161–175.

Magnus, W. and Oberhettinger, F. (1954). *Formulas and Theorems for the Functions of Mathematical Physics*, Chelsea Publ. Co., NY.

Mossakovskii, V. I. (1958). The pressure of a circular stamp on an elastic half-space whose modulus of elasticity is a power function of depth. *PMM* **22,** 123–125.

Oner, M. (1990). Vertical and horizontal deformation of an inhomogeneous elastic half-space. *International Journal of Numerical and Analytical Geomechanics* **14,** 613–629.

Rostovtsev, N. A. (1961). An integral equation encountered in the problem of a rigid foundation bearing on non-homogeneous soil. *PMM* **25,** 164–168.

Sneddon, I. N. (1946). Boussinesq's problem for a flat-ended cylinder. *Proceedings of the Cambridge Philosophical Society* **42,** 29–39.

Suresh, S., Giannakopoulos, A. E. and Alcala, J. (1996). Spherical indentation of compositionally graded materials: theory and experiments. *Acta Materials* (in press).

Yong, Y. and Hanson, M. T. (1994). Three-dimensional crack and contact problems with a general geometric configuration. *Journal of Mechanics and Physics of Solids* **42,** 215–238.

Yoffe, E. H. (1984). Modified Hertz theory for spherical indentation. *Philosophy Magazine, Series A* **50,** 813–828.

Whittaker, E. T. and Watson, G. N. (1962). *A Course of Modern Analysis*, Cambridge Publ., Cambridge, UK.

APPENDIX

Hruban (1958), Gibson and Kalsi (1974) and Calladine and Greenwood (1978) proved that a simple radial field exists in the case of $k = 1$ and $\nu = 0.5$ and follows the distribution of the homogeneous case. In a spherical coordinate system (R, θ, ϕ), it was found that the non-zero components of displacements, strains and stresses are

$$u_R = C/R^2, \quad \varepsilon_{RR} = -2C/R^3, \quad \varepsilon_{\theta\theta} = \varepsilon_{\phi\phi} = C/R^3, \quad \sigma_{RR} = \frac{-2CE_0 \cos\theta}{R^2}$$

with $C = 3P/(4\pi E_0)$. The displaced volume gives a remarkable relation between indentation displacement and contact stress, which are simply related with a Winkler type of spring constant of magnitude $2E_0/3$. It is clear that to keep surface displacements continuous, cylindrical punch cases should be avoided. The force-depth $(P-h)$,

radius-depth $(a-h)$ and contact pressure $p(r)$ relations for the spherical (parabolic) rigid indenter of diameter D take the form:

$$P = \frac{\pi}{3} D E_0 h^2, \quad h = \frac{a^2}{D}, \quad p(r) = \frac{2E_0}{3}\left(h - \frac{r^2}{D}\right).$$

Clearly, these cases show no sinking-in (or pile-up) of material and the displacements' derivatives are discontinuous at the contact perimeter. The same relations for the conical rigid indenter of half-apical angle α read as

$$P = \frac{2\pi^2}{9} (\tan\alpha)^2 E_0 h^3, \quad h = \frac{a}{\tan\alpha}, \quad p(r) = \frac{2E_0}{3} h\left(1 - \frac{r}{a}\right).$$